Ore Geology Reviews 67 (2015) 90–108

Contents lists available at ScienceDirect

Ore Geology Reviews

journal homepage: www.elsevier.com/locate/oregeorev

Spatial–temporal evolution of ore-forming fluids and related mineralization in the western Lanping basin, Yunnan Province, China

Jin-rang Zhang [a,b], Han-jie Wen [b,*], Yu-zhuo Qiu [b,c], Zhi-chao Zou [d], Sheng-jiang Du [b], Song-yang Wu [a]

[a] Chengdu Institute of Geology and Mineral Resources, China Geological Survey, Chengdu 610081, China
[b] State Key Laboratory of Ore Deposit Geochemistry, Institute of Geochemistry, Chinese Academy of Sciences, Guiyang 550002, China
[c] Key Laboratory for Metallogenic, Guangzhou Institute of Geochemistry, Chinese Academy of Sciences, Guangzhou 510640, China
[d] Chengdu University of Technology, Chengdu 610059, China

ARTICLE INFO

Article history:
Received 27 November 2013
Received in revised form 10 November 2014
Accepted 26 November 2014
Available online 3 December 2014

Keywords:
Cu–Ag–Pb–Zn polymetallic mineralization
Ore-forming fluids
Western Lanping basin
China

ABSTRACT

The Lanping basin is a significant Pb–Zn–Cu–Ag mineralization belt in the Sanjiang Tethyan metallogenic province. A series of sediment-hosted Himalayan Cu–Ag–Pb–Zn polymetallic deposits have been discovered in the western part of the basin, controlled by a thrust–nappe system. In the thrust–nappe system, the Cu orebodies mainly occur in the western and relatively deep part of the mineralization system (the root zone), whereas the Pb–Zn–Ag (±Cu) orebodies occur in the eastern and relatively shallow part of the system (the front zone), both as vein-type mineralization.

In this paper we present new data, combined with existing data on fluid inclusions, isotopes and geologic characteristics of representative deposits, to provide the first study that contrasts mineralizing fluids in the Cu–Ag (Mo) and Pb–Zn–Ag (Cu) polymetallic deposits.

Fluid inclusion and isotope studies show that the Cu–Ag (Mo) mineralization in the root zone formed predominantly from deep crustal fluids, with the participation of basinal brines. The deep crustal fluids are marked by high CO_2 content, relatively high temperatures (280 to 340 °C) and low salinities (1 to 4 wt.% NaCl equivalent), whereas the basinal brine shows relatively low temperatures (160 °C to 220 °C) and high salinities (12 to 22 wt.% NaCl equivalent), containing almost no CO_2. In comparison, hydrothermal activity associated with the Pb–Zn–Ag (±Cu) deposits in the front zone is characterized by basinal brine, with relatively low temperatures (130 °C to 180 °C), high salinities (9 to 24 wt.% NaCl equivalent), and low CO_2 concentrations. Although evolved meteoric waters have predominantly been proposed as the source for deep crustal fluids, magmatic and metamorphic components cannot be completely excluded. The basinal brine was predominantly derived from meteoric water.

The $\delta^{34}S$ values of sulfides from the Cu–Ag (Mo) deposits and Pb–Zn–Ag (±Cu) deposits range from −17.9 to 16.3‰ and from 2.5 to 11.2‰, respectively. These ranges may relate to variations in physicochemical conditions or compositional variation of the sources. Lead isotope compositions indicate that the ore-forming metals were predominantly derived from sedimentary rocks of the Lanping basin.

© 2014 Elsevier B.V. All rights reserved.

1. Introduction

The Lanping basin is located at the junction of the Eurasian and Indian Plates, in the eastern Tibetan Plateau, and is bordered by the Lancangjiang and Jinshajiang–Ailaoshan sutures (Fig. 1). The Lanping basin is a significant Pb–Zn–Cu–Ag mineralization belt in the Sanjiang Tethyan metallogenic province in China, which produces numerous economically significant deposits (He et al., 2009; Hou et al., 2006, 2008; Xue et al., 2002, 2003, 2007).

A series of Cenozoic base metal deposits occur in this basin, including the Jinding Zn–Pb deposit, which has a reserve of 200 Mt ore grading 6.08% Zn and 1.29% Pb, making it the largest sandstone-hosted Zn–Pb deposit in the world, and several Cu ± Ag ± Co deposits (Baiyangping, Baiyangchang and Jinman), mainly located in the northern segment of the basin (He et al., 2009; Hou et al., 2006, 2008; Khin et al., 2007; Xue et al., 2002, 2003, 2007). These deposits, with total reserves of more than 16.0 Mt Pb + Zn, 0.6 Mt Cu, and 7000 t Ag, are hosted by Mesozoic–Cenozoic mottled clastic rocks, and controlled by Cenozoic thrust systems related to the Indo-Asian collision since the Paleocene (He et al., 2004, 2009; Xu and Zhou, 2004). Spatially, these base metal deposits are divided into two sub-parallel metallogenic belts, which are characterized by sediment-hosted Cu–Ag polymetallic deposits in the western Lanping basin, and by Pb–Zn polymetallic deposits in the eastern Lanping basin (He et al., 2009; Hou et al., 2008; Xue et al., 2007).

In the western thrust–nappe system, the Pb- and Zn-poor Cu mineralization occurs as veins in the root zone, which is characterized by

* Corresponding author.
E-mail address: wenhanjie@vip.gyig.ac.cn (H. Wen).

http://dx.doi.org/10.1016/j.oregeorev.2014.11.017
0169-1368/© 2014 Elsevier B.V. All rights reserved.

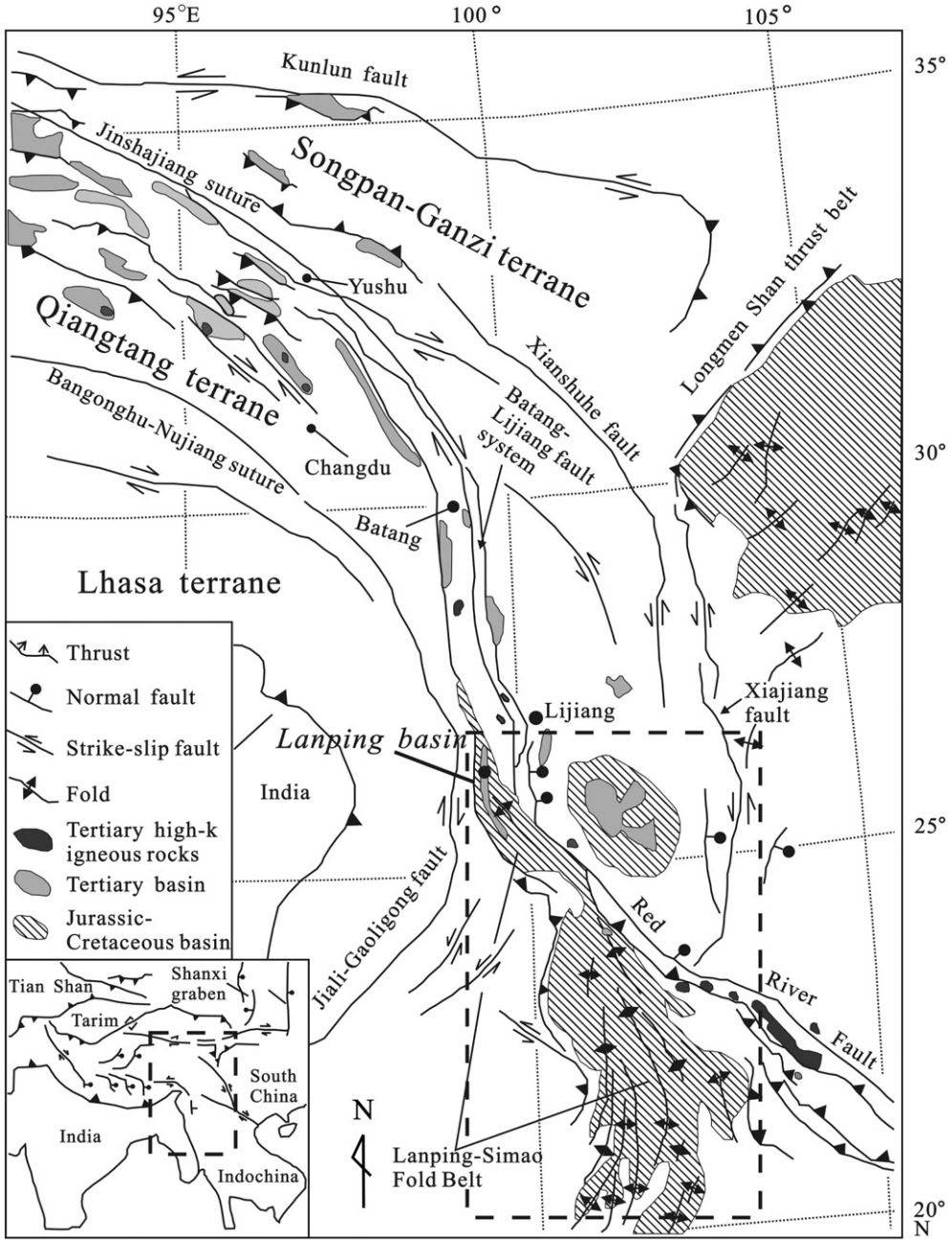

Fig. 1. Cenozoic tectonic map of eastern Tibet and Indochina, showing the major faults and the distribution of Mesozoic to Cenozoic basins (modified from He et al. (2009)).

high-angle west-dipping faults that juxtapose a Triassic carbonate sequence over Jurassic–Cretaceous strata. The Pb–Zn–Ag (±Cu) mineralization occurs in the front zone, which is characterized by a series of thrust faults that juxtapose Cretaceous strata over Tertiary strata. Over the last few decades, the genesis of these deposits in the western Lanping basin has been extensively studied (e.g., He et al., 2009; Hou et al., 2007, 2008; Kyle and Li, 2002; Luo and Yang, 1994; Qin and Zhu, 1991; Shi et al., 1983; Xue et al., 2003, 2007). However, debate continues concerning the absolute and relative timing and the origin of the Cu and Pb–Zn–Ag (±Cu) mineralization. The properties and evolution of the ore-forming fluid systems and depositional processes of the metals (Cu, Pb and Zn) still remain uncertain (He et al., 2009; Hou et al., 2006; Wu et al., 2003; Xue et al., 2007; Zhang et al., 2002).

It has been previously proposed that the Cu and Pb–Zn deposits were contemporaneous with, or immediately followed thrust–nappe deformation in the western Lanping basin, and originated in the same fluid-flow system (He et al., 2009; Hou et al., 2008; Li and Fu, 2000; Liu et al., 2000; Wu et al., 2003; Xiao et al., 1994; Yan and Li, 1997). Most of the previous geochemical studies proposed that the ore-forming materials and fluids were mainly derived from the basin (He et al., 2009; Li and Fu, 2000; Liu et al., 2000; Wu et al., 2003; Xiao et al., 1994; Yan and Li, 1997), whereas some studies argued that the ore-forming components were mainly derived from the mantle or magmatic intrusions through deep structures (Chi and Xue, 2011; Ji and Li, 1998; Que et al., 1998; Xue et al., 2003). Several recent studies, however, revealed that the Cu and Pb–Zn orebodies precipitated from different fluid-flow systems in multiple mineralization episodes (Song et al., 2011; Xu and Zhou, 2004; Zhao, 2006).

In this paper we present new data, and review existing geology, fluid inclusion, isotope geochemistry, and geochronology data of

representative Cu and Pb–Zn deposits, and provide new observations on the spatial and temporal relationships between Cu and Pb–Zn mineralization. Furthermore, we provide the first description of the properties and spatial–temporal evolution of ore-forming fluids in the western Lanping basin, as well as their related mineralization. On the basis of fluid inclusion analyses, isotope studies, and geologic characteristics, we postulate that the Cu–Ag (Mo) mineralization in the root zone is dominated by deeply-circulating meteoric water. In comparison, hydrothermal activity associated with the Pb–Zn–Ag (Cu) deposits in the front zone is characterized by basinal brine. The ore-forming metals, both for the Cu–Ag (Mo) deposits and the Pb–Zn–Ag (Cu) deposits, are predominantly derived from sedimentary rocks in the basin. Our study provides new constraints on ore genesis for the deposits examined, as well as for other deposits in the western Lanping basin.

2. Geological setting of the Lanping basin

The Lanping–Simao foreland fold belt (Fig. 1), a NNW-trending intra-continental basin, is located in the eastern Indo-Asian collision zone (EIACZ). This basin is confined by the Jinshajiang–Ailaoshan suture to the east, and the Lanchangjiang suture to the west (Fig. 1; He et al., 2009; Hou et al., 2008; Xue et al., 2002, 2007). Tectonically, it is located on the border of the Yangtze Plate to the east, and the Tibet Plate to the west (He et al., 2009; Hou et al., 2008; Xue et al., 2002, 2007). The basement of the Lanping–Simao foreland fold belt consists primarily of Proterozoic and Paleozoic strata (He et al., 2009; Xue et al., 2007). The Proterozoic metamorphic basement rocks (i.e., sericite schist, marble, gneiss) are distributed along the margins of the Lanping–Simao basin, and are similar to those that underlie the Yangtze Plate (Mu et al., 1999; Xue et al., 2007).

The Lanping basin, as a part of the Lanping–Simao fold belt, is filled with Mesozoic and Cenozoic strata to more than 10 km thick. The Mesozoic and Cenozoic strata are mainly continental siliciclastic rocks, except for the lowest part of the sequence and the Upper Triassic Sanhedong Formation (T_3s), which mainly consist of marine limestone (Xue et al., 2002, 2007). The Mesozoic–Cenozoic strata (Fig. 2) that outcrop in the Lanping basin are summarized as follows. The Mesozoic strata comprise the Upper Triassic Sanhedong Formation (T_3s) composed of marine carbonate rocks, the Middle Jurassic Hakaizuo Formation (J_2h) composed of carbonate-bearing sandstone and carbonaceous shale/slate, and the Lower Cretaceous Jingxing Formation (K_1j) composed of terrestrial red clastic rocks.

The outcrops of Himalayan igneous rocks are mostly restricted to the margins of the Lanping basin. Only a few igneous rocks occur inside the southern basin, such as the Zhuopan and Huanglianpu intrusives in Yongping County, and the Weishan intrusive in Weishan County (Fig. 1; Xue et al., 2002, 2007). The lithology of the intrusive rocks

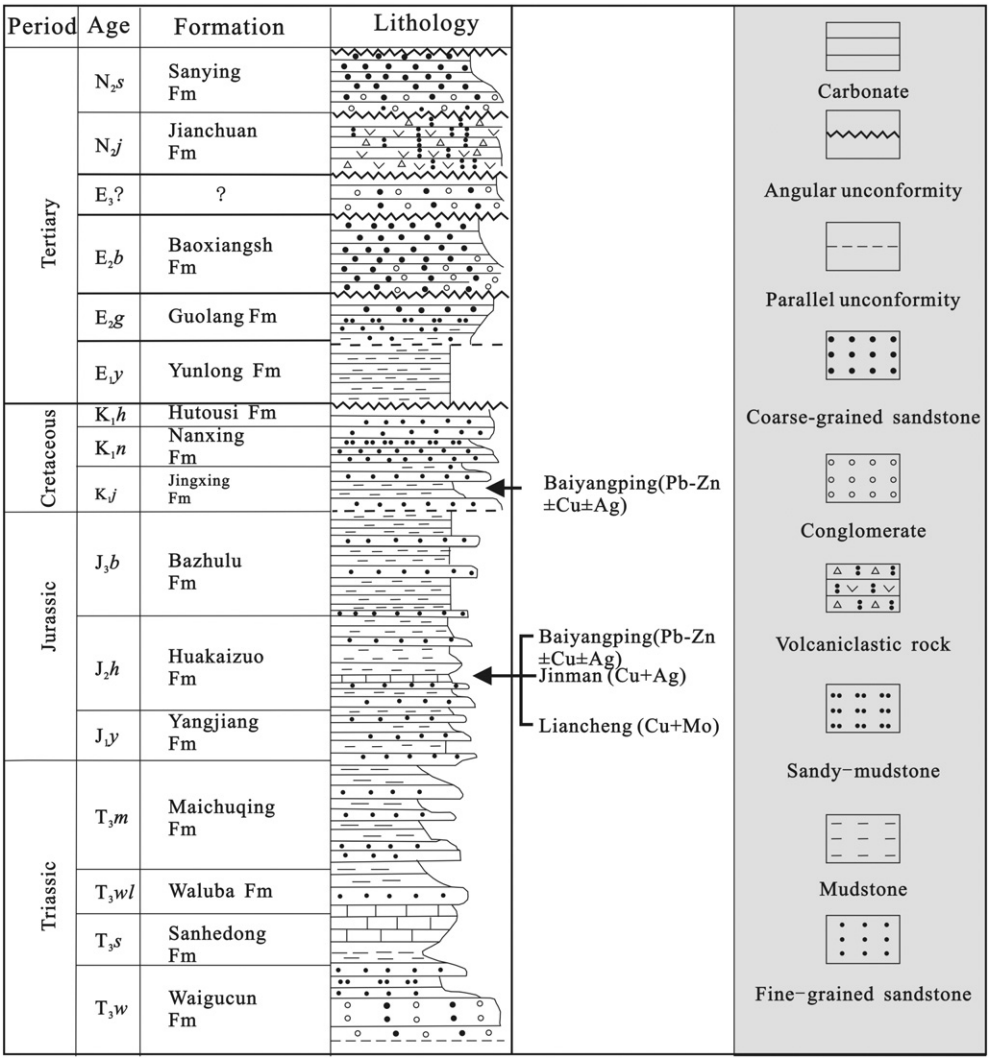

Fig. 2. Stratigraphic units in the Lanping basin (modified from Mu et al. (1999)).

include quartz syenite, quartz monzonite porphyry, granitic porphyry and nepheline monzogabbro, with ages ranging from 68 Ma to 23 Ma (Rb–Sr, U–Pb, and Ar–Ar methods; Dong et al., 2005; Xue et al., 2002; Zhang et al., 2000; Zhao, 2006). Geochemical characteristics indicate that these Cenozoic magmatic rocks are of mantle origin (Xue et al., 2007). No magmatic rock occurs on the surface in any of the mineralization areas, although Zhang et al. (2000) proposed a giant magmatic belt concealed in the western Lanping basin, as revealed by gravity and remote sensing data.

Dynamic processes in the Lanping basin were controlled by the trans-lithosphere faults along the basin margins and the crust-penetrating faults in the middle of the basin (Fig. 3a, Xue et al., 2002; Zhang et al., 2000). The tectonic evolution of this basin was complex, with rifting during the Indosinian epoch (rift basin), depression during the Yanshanian epoch (continental depression basin), and strike-slip extension during the Himalayan epoch (continental pull-apart basin) (Xue et al., 2002).

3. Distribution and characteristics of mineral deposits

As a consequence of the Indo-Asian collision (beginning at ~65 Ma; Hou et al., 2008), two large-scale Cenozoic thrust–nappe systems superposed the Mesozoic strata over the Tertiary strata in the Lanping basin, and dominated the spatial distribution of Cenozoic Pb–Zn–Cu–Ag deposits. More than 100 thrust-controlled, sediment-hosted, Himalayan Pb–Zn deposits (Jinding), as well as several Cu ± Ag ± Co deposits (Baiyangping, Baiyangchang and Jinman) have been discovered, mostly in the northern part of the basin (He et al., 2009; Hou et al., 2006, 2008; Khin et al., 2007; Xue et al., 2007). Spatially, the mineralization occurs in two sub-parallel metallogenic belts, separated by the central–axial Lanping–Simao fault (Xu and Zhou, 2004; Xue et al., 2003). The mineralization belts are characterized by vein-type Cu polymetallic deposits in the western thrust–nappe system (e.g., the Jinman Cu deposit, the Liancheng Cu–Mo deposit and the Baiyangping Cu–Ag–Co deposit), and Pb–Zn–Ag–Cu deposits in the eastern thrust–nappe system (e.g., the Jinding Zn–Pb deposit and the Sanshan Ag–Pb–Zn deposit) (Fig. 3b, He et al., 2009; Hou et al., 2008; Xue et al., 2007).

In the western thrust–nappe system, the Pb- and Zn-poor Cu orebodies occur as vein-type deposits in the root zone, mainly hosted in Jurassic variegated clastic rocks. Copper, Mo, and Ag are the predominant commodities in the root zone, including the Jinman Cu–Ag deposit, Liancheng Cu–Mo deposit, and more than 30 small vein copper deposits such as Kedengjian, Huangbai, and Enqi (He et al., 2009; Li and Fu, 2000; Xu and Zhou, 2004). The Pb–Zn–Ag (Cu) deposits, controlled by second-order faults of major thrust faults, are mainly distributed in the front zone, including the Baiyangping Cu–Ag–Pb–Zn ore belt, and some small Ag-bearing Pb–Zn deposits, such as Liziping and Wudichang (Fig. 3b, He et al., 2009; Xue et al., 2010). The geologic and mineralogical features of these typical deposits (Table 1) have been described by Hou et al. (2008) and He et al. (2009). Features of some representative deposits are briefly described in what follows.

3.1. The Baiyangping Cu–Ag–Pb–Zn ore belt

The Baiyangping Cu–Ag–Pb–Zn ore belt (Fig. 4), consisting of two blocks (the Fulongchang and Baiyangping blocks), is an important member of the western metallogenic belt in the Lanping basin. It is located in the front zone, about 30 km northwest of Jinding (Fig. 3b). It contains ~2000 t Ag, 0.12 Mt Cu and minor reserves of Zn and Pb (Table 1). At the scale of the ore zone, three groups of faults can be distinguished, including the N-S-striking Sishiliqing thrust fault and its second-order faults (F_6–F_9, F_{12}), and the ~E-W trending strike-slip fault F_5. The Baiyangping and Fulongchang blocks mainly occur in the second-order faults F_6–F_9 and F_{12} (Fig. 4).

The orebodies are mainly hosted in the Cretaceous Jinxing Formation (K_1j) sandstone, siltstone, and mudstone, and partially in the siliceous mudstone of the Middle Jurassic Huakaizuo Formation (J_2h). Mineralization in the Baiyangping ore belt is dominated by pore filling and cementation, and ore structures are dominated by veinlet, network and breccia structures.

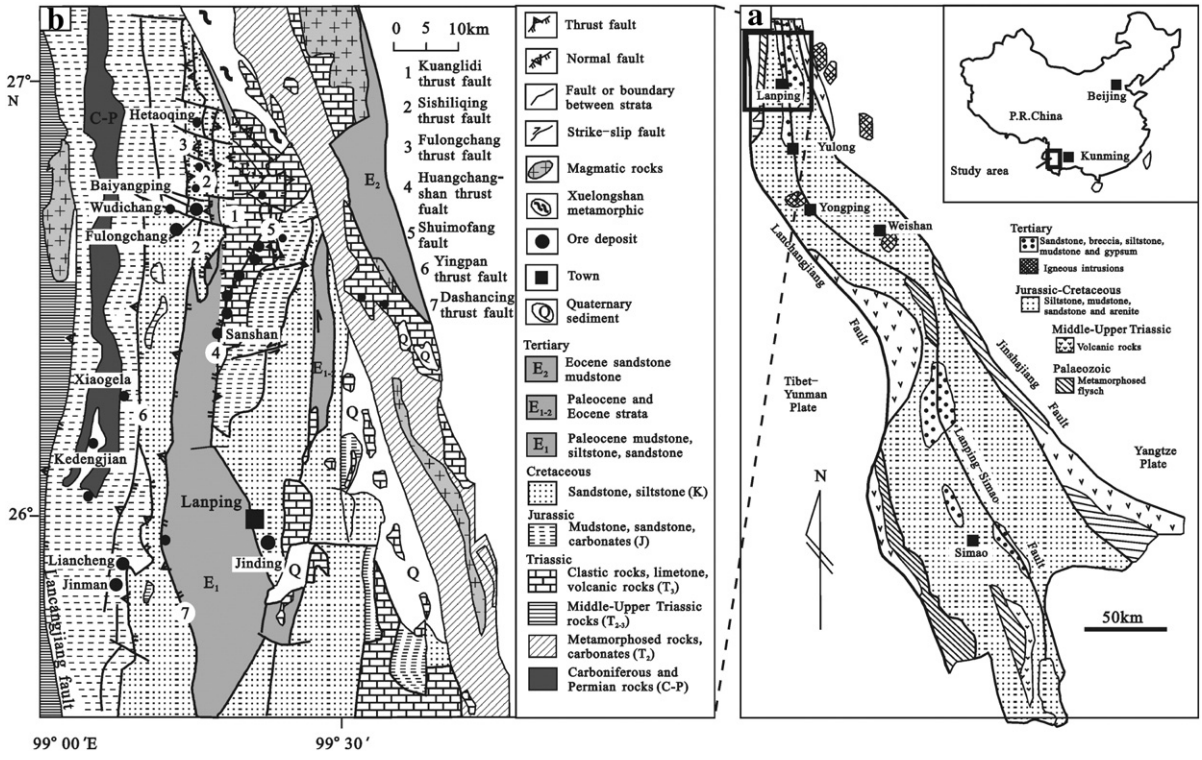

Fig. 3. (a)—Sketch geological map of the Lanping–Simao foreland fold belt, China; (b)—Distribution map of main deposits in the northern Lanping basin (modified after Xue et al. (2007)).

Table 1
Summary of geological and mineralogical features of economically significant deposits in the Lanping foreland fold belt.

Deposit	Structural location	Wall rock	Grade and tonnage	Sulfide assemblages	Economic metals	Data source
Jinding	The eastern thrust–nappe system	K_1j: sandstone and arenite; E_1y: breccia, sandstone and gypsum	Pb:64 Mt; 1.16–2.42%,Zn:12.84 Mt; 8.32–10.52%Ag: 1722 t; 12.5–12.6 g/t	Gn, Sp, Py,Mrc, Clt,Sm	Zn–Pb	Xue et al. (2007)
Sanshan	The front zone of the eastern thrust–nappe system	T_3s: limestone and limestone; E_1y and E_2b: sandstone	Zn + Pb: 0.5 MtAg: 3000 tCu: ~0.3 Mt	Ttr, Ar, Py, Az, Ccp Sp, Gn	Ag–Pb–Zn–Cu	He et al. (2009)
Fulongchang	The front zone of the western thrust–nappe system	K_1j: sandstone and arenite; J_2h: quartz sandstone and mudstone	Ag: 2000 t, 328–547 g/t; Cu: 0.1 Mt, 0.63–11.70%; Pb: 4.2–7.4%	Ttr, Py, Ccp, Gn, Fre	Cu–Ag–Pb–Zn	Chen et al. (2000); Zhao (2006)
Baiyangping	The front zone of the western thrust–nappe system	K_1j: sandstone and arenite; J_2h: quartz sandstone and mudstone	Ag: 3.0–33.8 g/t; Cu: 0.86–3.3%;Co: 0.10–0.27%	Ttr, Py, Ccp, Gn, Fre	Cu–Ag–Co	Chen et al. (2000); Zhao (2006)
Wudichang	The front zone of the western thrust–nappe system	J_2h: mudstone, sandstone, and carbonates	Pb: 4.2–10.4%,Zn: 12.2–15.33%	Sp, Gn, Py, Ar	Pb–Zn–Ag	Song et al. (2011)
Liziping	The front zone of the western thrust–nappe system	J_2h: mudstone, sandstone, and carbonates	Pb: 1.96–57.19%,Zn: 2.37–30.26%Ag: 17.7–1176.2 g/t	Sp, Gn, Py	Pb–Zn–Ag	Kong and Qi (2009); Zou 2012
Jinman	The root zone of the western thrust–nappe system	J_2h: quartz sandstone, mudstone, carbonaceous shale, and slate	Cu: >0.2 Mt, 2.58%; minor Ag, ~100 g/t	Ttr, Ccp, Bn, Cct, Py	Cu–Ag	Li and Fu (2000); Zhao (2006)
Liancheng	The root zone of the western thrust–nappe system	J_2h: quartz sandstone, mudstone, carbonaceous shale, and slate	Under exploration	Ttr, Mol,Ccp, Bn, Cct, Py	Cu–Mo	Li and Fu (2000); Zhao (2006)

[a] Ore mineral abbreviations (Whitney and Evans, 2010). Ar: argentite, Az: azurite, Bn: bornite, Cct: chalcocite, Clt: celestine, Ccp: chalcopyrite, Fre: freibergite, Gn: galena, Mrc: marcasite, Mol: Molybdenite, Py: pyrite, Sm: smithsonite, Sp: sphalerite, Ttr: tetrahedrite. [b] Strata abbreviations. E_2b: Eocene Baoxiangsi Formations; E_1y: Palaeocene Yunlong Formation; K_1j: Lower Cretaceous Jingxing Formation; J_2h: Middle Jurassic Huakaizuo Formation; T_3s: Upper Triassic Sanhedong Formation.

Ore minerals are dominated by tetrahedrite, arsenian tetrahedrite, sphalerite, galena, argentite, chalcopyrite, and minor native silver (He et al., 2009; Zhao, 2006). Silver is mainly present as native silver, with minor amounts in tetrahedrite and argentite (Zhao, 2006). Gangue minerals associated with mineralization include calcite, siderite, barite, and minor quartz (He et al., 2009).

3.2. The Jinman Cu–Ag deposit

The Jinman deposit (Fig. 5a, c) is the largest and highest grade Cu deposit in the root zone of the western thrust–nappe system (Fig. 3b). It has a reserve of 7.75 Mt ore with average grade of 2.58% Cu (under exploration), mainly hosted in Jurassic strata (He et al., 2009; Hou et al., 2008). The deposit is controlled by a NNE-striking compressive fault, which probably resulted from regional eastward thrusting (Hou et al., 2006). The main ore-hosting strata are a suite of terrestrial–marine low-grade metamorphic rocks composed of schist, sandy slates, and mudstones of the Middle Jurassic Huakaizuo Formation. The wall rock alteration associated with mineralization is characterized by weak silicification and carbonatization, which mainly produce siliceous rocks, and veins of quartz, calcite, and dolomite, with minor siderite. The mineralization is dominated by sulfide-bearing quartz–calcite veins, although disseminated orebodies in altered wall rocks are also common. The veins are generally parallel to

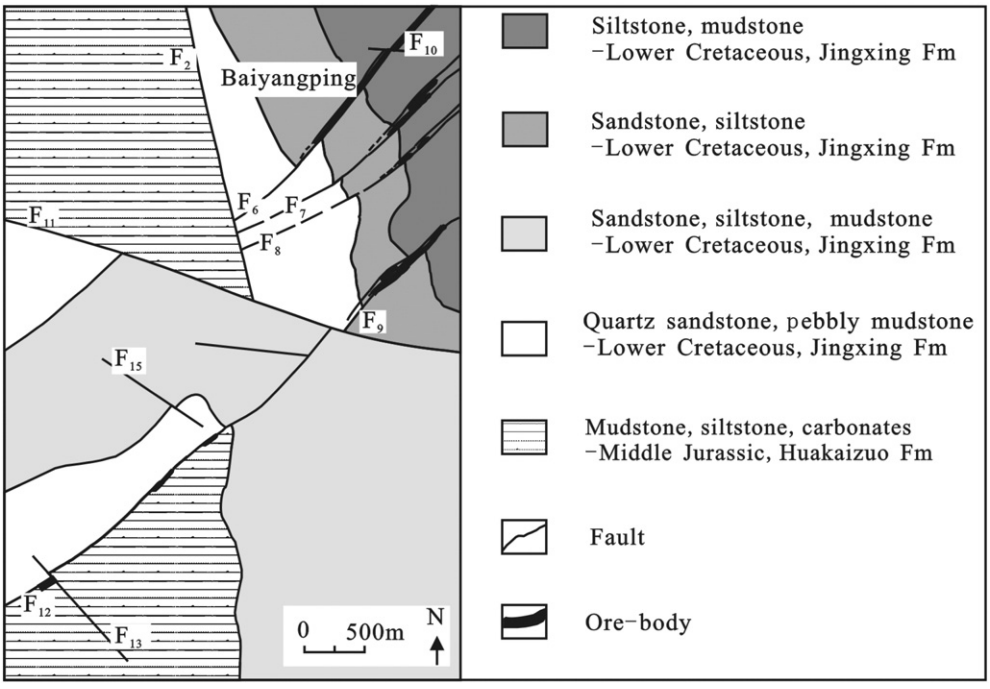

Fig. 4. Simplified geologic map of the Baiyangping ore belt (modified from He et al. (2009)).

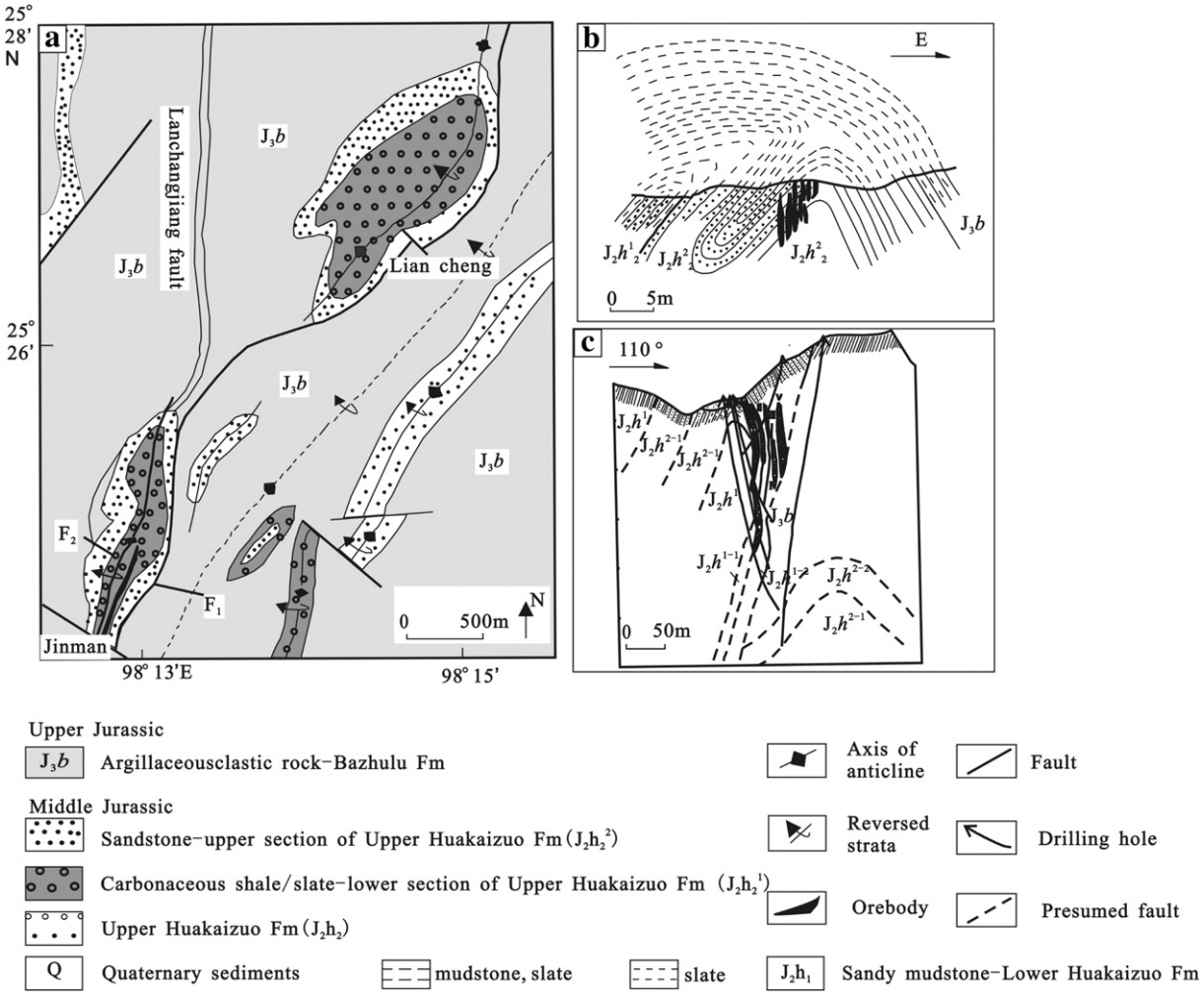

Fig. 5. (a) Geologic map of the Jinman and Liancheng deposits, (b) a cross-section through the ore body of the Liancheng deposit and, (c) a cross-section through the ore body of the Jinman deposit (modified from Li and Fu (2000)).

bedding, with thicknesses ranging from tens of centimeters to a few millimeters (Fig. 6a–d) (Li and Fu, 2000; Liu et al., 2000).

Ore minerals are dominated by tetrahedrite, Ag-bearing tetrahedrite, chalcopyrite, bornite and chalcocite (Fig. 6a–d). Small amounts of pyrite, sphalerite, and galena are also present. Gangue minerals include quartz, calcite, ankerite, barite, and minor sericite (He et al., 2009; Hou et al., 2008; Liu et al., 2001).

On the basis of mineralization features, cross-cutting, and paragenetic relationships, the Jinman mineralization can be divided into three stages: (I) quartz + ankerite + minor chalcopyrite + tetrahedrite + bornite + minor pyrite, (II) quartz + calcite + chalcopyrite + bornite + tetrahedrite + minor ankerite + minor pyrite, and (III) quartz + calcite + minor chalcopyrite, chalcocite, covellite and bornite stage (He et al., 2009; Zhao, 2006).

3.3. The Liancheng Cu–Mo deposit

The Liancheng Cu–Mo polymetallic deposit (Fig. 5a, b) is located in the root zone of the western thrust–nappe system (Fig. 3b), only ~2 km northwest of Jinman (Li and Fu, 2000). This deposit is controlled by the same structures as the Jinman deposit. The main ore-hosting strata are also a suite of terrestrial–marine low-grade metamorphic rocks composed of the Middle Jurassic Huakaizuo Formation schist, sandy slates, and mudstones. The wall rock alteration is characterized by weak silicification and carbonatization. The orebodies are mainly hosted in the Middle Jurassic Huakaizuo Formation mottled clastic rocks, schist, sandy slates, and mudstones. The mineralization in the deposit is mainly veins, with minor stratiform or lenticular bodies. Ore-bearing quartz and calcite vein systems are widespread in the Lancheng deposit, most of which occur parallel to the bedding of wall rock (Li and Fu, 2000; Zhao, 2006).

Ore minerals are dominated by tetrahedrite, chalcopyrite, molybdenite, bornite, chalcocite, and minor pyrite. Gangue minerals include quartz, calcite, ankerite, and minor siderite (Fig. 6e–f, Li and Fu, 2000; Zhao, 2006). Based on paragenetic studies, the ore-forming process can be divided into early, middle, and late stages, characterized by quartz–molybdenite veins, quartz–copper sulfide veins and carbonate veins, respectively (Fig. 6e–f; Li and Fu, 2000; Zhao, 2006; Zhang et al., 2012).

4. Fluid inclusion studies

4.1. Analytical methods

Microthermometric data for fluid inclusions from the deposits in the western Lanping basin have been reported by numerous previous studies, but the nature and evolution of the ore-forming fluids still remain uncertain (Chi and Xue, 2011; Ji and Li, 1998; Que et al., 1998; Xu and Zhou, 2004; Yan and Li, 1997). On the basis of the previous results, we systematically investigated the fluid inclusion characteristics of representative deposits (i.e., Jinman, Liancheng and Baiyangping). Doubly

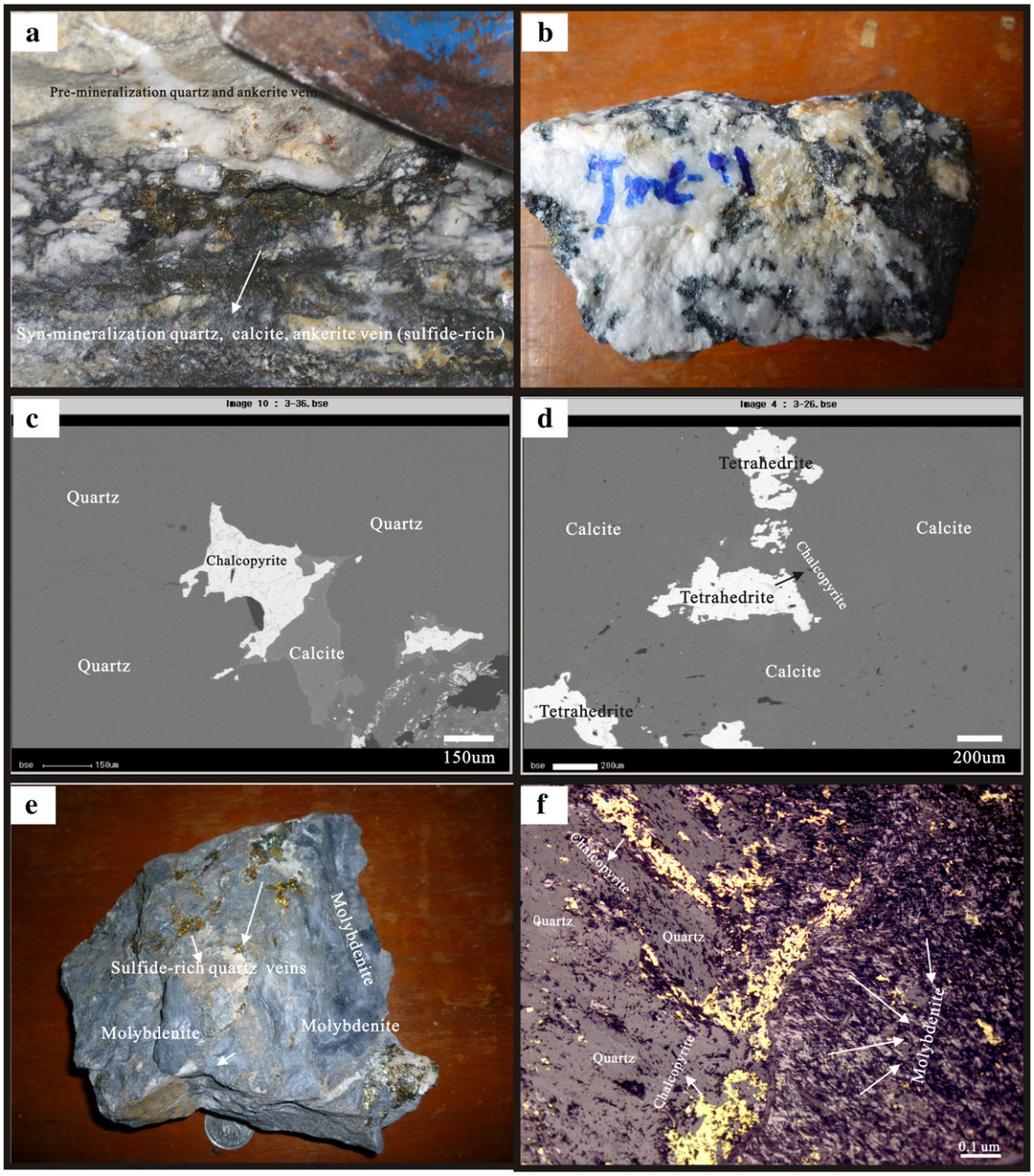

Fig. 6. Scanned pictures of ores and photomicrographs showing relationships of hydrothermal minerals in the Jinman and Liancheng deposits. a. Syn-mineralization quartz and calcite veins (bearing some copper sulfides) cutting pre-mineralization quartz and ankerite vein. b. Sulfide-rich quartz and calcite vein. c. Back-scattered electron (BSE) image of quartz that is cut by chalcopyrite-bearing quartz veinlets. d. Back-scattered electron (BSE) image of chalcopyrite and tetrahedrite in the syn-mineralization calcite. e. Early molybdenite cut by quartz–sulfide veins. f. Early fibrous molybdenite cut by quartz–sulfide vein.

polished sections were prepared from 18 representative samples of these deposits. Fluid inclusion observations were performed on a standard polarization microscope to define successive assemblages of fluid inclusions and to document their paragenetic relationships to ore minerals. Fluid inclusion microthermometry was performed at the Institute of Geochemistry, Chinese Academy of Sciences (IGCAS) in Guiyang, China, on a Linkam THMSG 600 programmable heating–freezing stage attached to a Leica microscope. The equipment was calibrated using synthetic fluid inclusions. Estimated accuracy is about ±0.2 °C for temperatures below 50 °C and ±2 °C above 100 °C (Su et al., 2009). Total salinities for aqueous fluid inclusions were calculated from final melt temperatures according to Bodnar (1993), and were expressed as wt.% NaCl equivalent. The salinities of the CO_2–H_2O inclusions were calculated from the melt temperature of clathrate (Roedder, 1984).

4.2. Petrography and microthermometric measurements

The ore-forming fluids responsible for Cu–Ag (Mo) mineralization in the root zone are characterized by three types of primary fluid inclusions: aqueous (type A), H_2O–CO_2 (type B), and CO_2-dominated (type C). Type A inclusions consist of aqueous solution and water vapor, and generally have a degree of fill of about 50% to 90% (mainly 70% to 80%) (Fig. 7b, e, f). Type B inclusions comprise aqueous solution and single- or two-phase CO_2, which can be further divided into type B-1, consisting of two (aqueous + carbonic) phases (Fig. 7d, e; Fig. 8), and type B-2 consisting of three (aqueous + liquid carbonic + vapor carbonic) phases (Fig. 7a, c, e, f). Type C inclusions contain one or two carbonic phases (mainly CO_2), without a visible aqueous phase (Fig. 7a, b, e, f). The fluid inclusions types generally appear separately

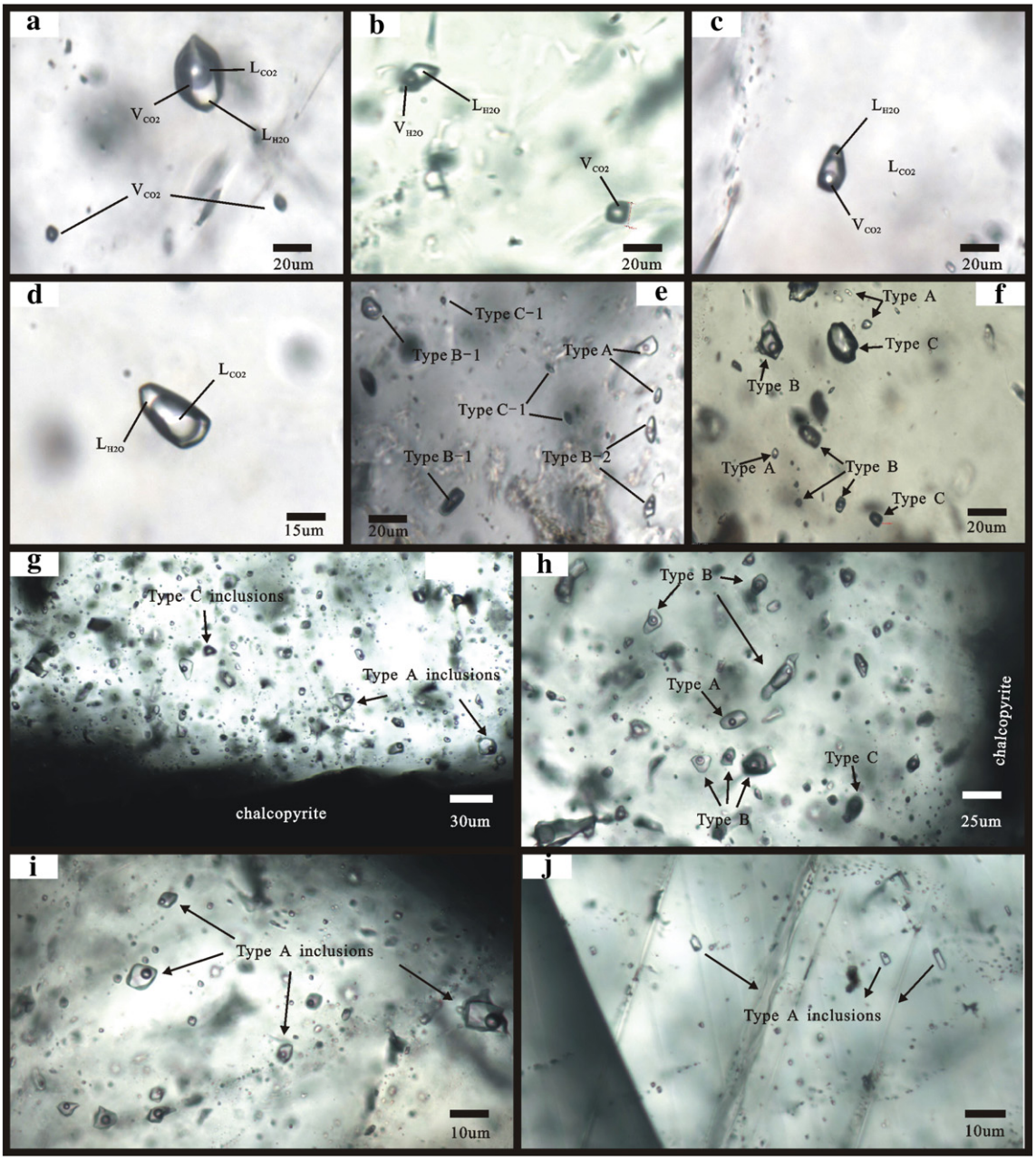

Fig. 7. Photomicrographs of fluid inclusion at 25 °C at the base metal deposits in the western Lanping basin. (a). Type B-2 inclusions occurring together with C inclusions in quartz from the Liancheng deposit. (b). Type B-1 inclusions occurring together with C inclusions in quartz from the Liancheng deposit. (c). Type B-2 occurring alone in quartz from the Liancheng deposit. (d). Type B-1 occurring alone in quartz from the Liancheng deposit. (e). Type A, B, and C inclusions coexisting together within a small area at the Liancheng deposit. (f). Type A, B, and C inclusions coexisting together within a small area at the Liancheng deposit. (g). Several type A inclusions and minor type C inclusions occurring near chalcopyrite at Jinman deposit. (h). Type A, B, and C inclusions coexisting together within a small area adjacent to chalcopyrite at the Jinman deposit. (i). A series of type A inclusions occurring together in quartz at from the Baiyangping ore belt. (j). Some type A inclusions in calcite from the Baiyangping ore belt.

in these Cu–Ag (Mo) deposits. However, it is also common to see type B fluid inclusions, with various volume proportions of the CO_2 phase, coexist with type A and type C inclusions in groups at the Jinman Cu deposit and the Liancheng Cu–Mo deposit (Fig. 7e–h).

In contrast, the ore-forming fluids responsible for the Pb–Zn–Ag (Cu) deposits in the front zone are characterized by aqueous (type A) inclusions only (Fig. 7i–j, Xu et al., 2005; Xue et al., 2010).

Microthermometric data, together with some previously published, are summarized in Table 2, and graphically presented in Figs. 9, 10. For the Cu–Ag (Mo) deposits in the root zone, the CO_2 melting temperatures ($T_{m\text{-}CO2}$) in CO_2-bearing inclusions for all deposits range from −58.3 °C to −56.3 °C, suggesting that the carbonic phase is approximated by CO_2, with only minor amounts of other volatiles. This result has been well confirmed by Laser Raman analysis (Fig. 8, Xu et al., 2005; Zhang et al., 2012). The partial homogenization temperatures ($T_{h\text{-}CO2}$) of the CO_2 phase, mostly homogenizing into the liquid phase, range from 20.8 °C to 30.1 °C, corresponding to densities of 0.59–0.76 g/cm^3.

At the Jinman deposit, the type B inclusions in both pre-ore and syn-ore quartz yield similar total homogenization temperatures ($T_{h\text{-}tot}$) in the range of 224–334 °C, although they show obviously different homogenization behaviors, homogenizing into liquid (aqueous phase) or vapor (carbonic phase). The clathrate melting temperatures ($T_{m\text{-}clath}$) of type B inclusions range from 7.6° to 9.8 °C, corresponding to salinities that range from 0.4 to 4.6 wt.% NaCl equivalent. However, the microthermometric parameters of aqueous inclusions (type A) show significant differences between pre-ore and syn-ore quartz. The type A

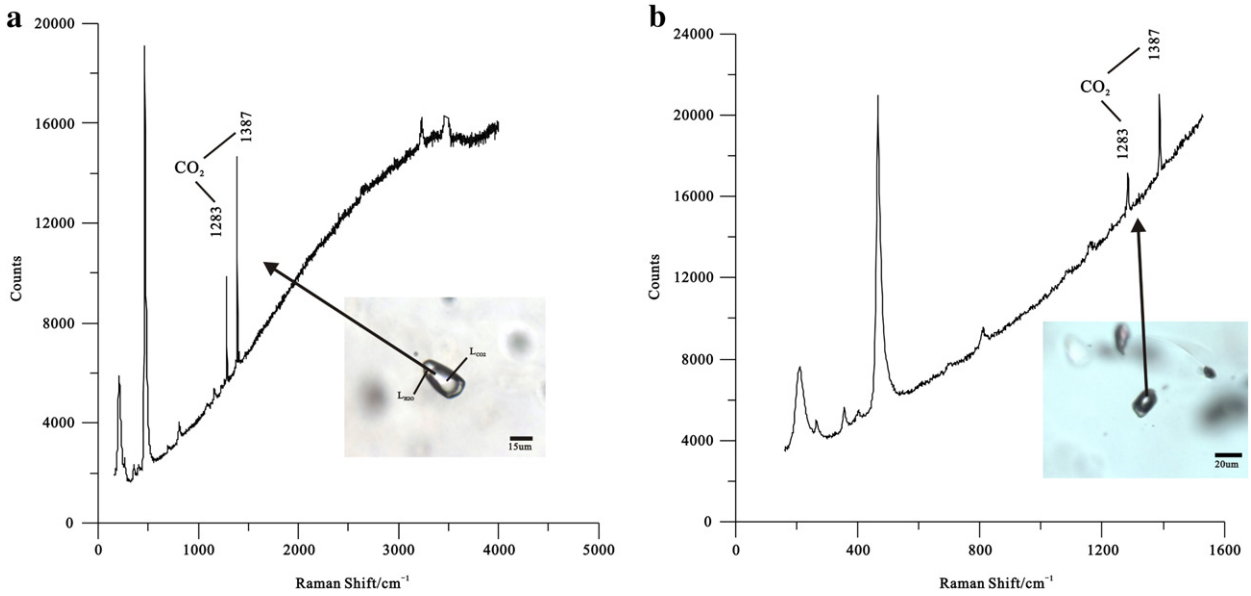

Fig. 8. Laser Raman spectra of Type B1 fluid inclusions. a. Data from the Liancheng Cu–Mo deposit; b. data from the Jinman Cu deposit.

fluid inclusions in the pre- and syn-ore quartz have homogenization temperatures of 143–236 °C and 116–239 °C, respectively, with medium salinities of 3.1 to 18.0 wt.% NaCl equivalent and 3.9 to 22.8 wt.% NaCl equivalent, respectively.

At the Liancheng deposit, mineralization can be subdivided into three stages, for which the type A fluid inclusions yield homogeneous temperatures of 236–346 °C, 176–229 °C, and 120–185 °C, respectively, with salinities of 9.0–22.3 wt.% NaCl equivalent, 7.2–21.3 wt.% NaCl equivalent, and <9.0 wt.% NaCl equivalent, respectively. The type B fluid inclusions of the early and middle mineralizing stages have homogeneous temperatures of 240–343 °C and 228–288 °C, respectively, with similar, low salinities of 0.6–4.1 wt.% NaCl equivalent.

For the Pb–Zn–Ag (±Cu) deposits in the front zone, primarily aqueous inclusions developed and only a few CO_2-bearing inclusions have been found (He et al., 2009; Xu et al., 2005; Xue et al., 2010). At the Baiyangping Cu–Ag–Pb–Zn ore belt, the homogenization temperature values ($T_{h\text{-}tot}$) for aqueous inclusions range from 110 to 283 °C (concentrating on a range of 130 to 180 °C), and the corresponding salinities vary from 3.9 to 24.3 wt.% NaCl equivalent (concentrating on a range of 9 to 24 wt.% NaCl equivalent) (e.g., He et al., 2009; Xu et al., 2005; Xue et al., 2010). Previously published initial ice-melting temperature values (T_e) range from −51.6 °C to −52.3 °C (Xue et al., 2010), similar to the eutectic melting temperature in H_2O–NaCl–$CaCl_2$ (Lu et al., 2004), indicate a H_2O–NaCl–$CaCl_2$ brine system.

5. Isotope geochemistry

5.1. Analytical techniques

All samples were crushed, sieved, and finally handpicked under a binocular microscope to a purity of greater than 99%. The H and O isotopic compositions of quartz were determined on a Finnigan MAT 251 mass spectrometer at the Key Laboratory of Isotope Geology, Ministry of Land and Resources, Beijing. The analytical precision in this study is better than 2‰ for H, and 0.2‰ for O isotopic compositions (2σ). Additional details of analytical procedures can be found in Tian et al. (2006). The S isotopic compositions were analyzed on a MAT 251 mass spectrometer at the Key Laboratory of Ore Deposit Geochemistry, Institute of Geochemistry, Chinese Academy of Sciences, Guiyang. The analytical precision is better than 0.2‰. Isotopic data are relative to standard mean ocean water (SMOW) for O and H, and to the Canyon Diablo Troilite (CDT) for S.

Table 2
Fluid inclusion types and microthermometric data from base metal deposits in the western Lanping basin.

Deposits	Material	Type	$T_{m,CO2}$ (°C)	$T_{m,cla}$ (°C)	$T_{h,CO2}$ (°C)	T_h (°C)	Salinity (wt.% NaCl eq.)	Reference
Jinman	Pre-ore quartz	Type A				143 ~ 236	3.1 ~ 18.0	This study
		Type B	−57.1–−56.8	7.8–9.6 °C	21.8–30.1	224–334	0.8–4.3	
		Type C			20.8–29.7			
	Syn-ore quartz	Type A				116–239	4.1–22.8	
		Type B	−57.8–−56.7	7.6–9.8 °C	22.1–30.1	217–327	0.4–4.6	
		Type C			21.8–29.6			
Liancheng	Early-stage quartz	Type A				236–346	9.0–22.3	
		Type B	−57.8–−56.4	7.9–9.7 °C	21.1–30.1	240–343	0.6–4.1	
		Type C			25.8–30.1			
	Middle-stage quartz	Type A					7.2–21.3	
		Type B	−58.3–−56.3	8.1–9.6 °C	22.7–30.1	176–229	0.8–3.7	
		Type C			27.8–29.7	228–288		
	Late-stage quartz/calcite	Type A				120–185	1.4–9.3	
Baiyangping	Main	Type A				110–283	3.9–24.3	Xue et al. (2010)

$T_{m,CO2}$—melting temperature of CO_2; $T_{m,cla}$—melting temperature of CO_2 clathrate; $T_{h,CO2}$—partial homogenization temperature of CO_2 inclusions; T_h—total homogenization temperature of inclusions; T_{ice}—freezing temperature.

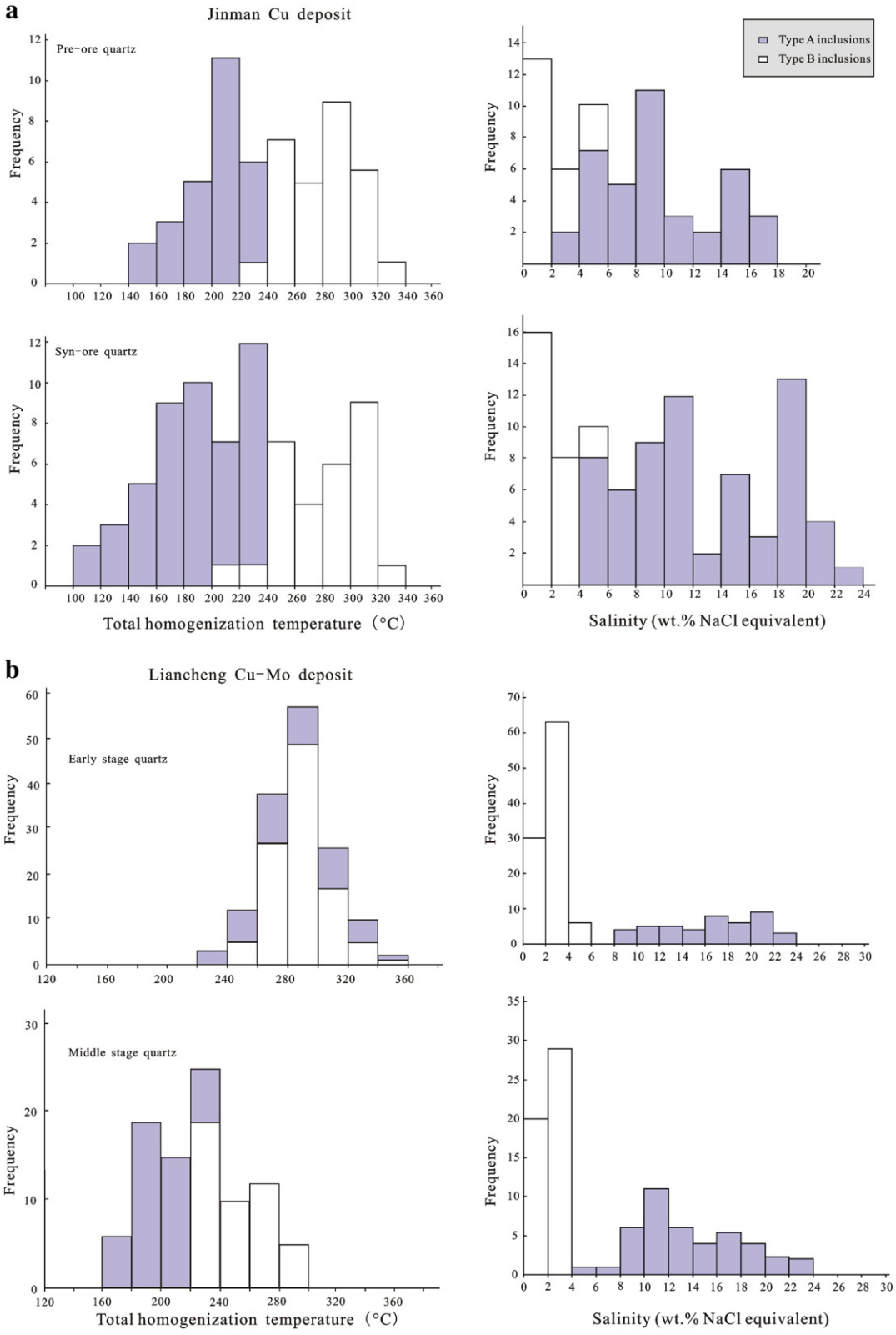

Fig. 9. Histograms of microthermometric data of fluid inclusions. a. Data from Jinman Cu deposit; b. data from Liancheng Cu–Mo deposit.

For the He and Ar isotopic measurements, we carefully selected chalcopyrites and pyrites from ore-bearing quartz veins that contain the fewest secondary fluid inclusions, to minimize the involvement of secondary inclusions in the analysis. All the samples were prepared and analyzed at the Laboratory of Gas Geochemistry, Lanzhou Institute of Geology, Chinese Academy of Sciences. All samples, packed with aluminum foils, were shifted to the crucible for gas extracting under high vacuum conditions. When a pressure lower than 1×10^{-5} Pa was attained, the samples were heated at 130 °C for at least 10 h to eliminate secondary fluid inclusions and trace gases, and then fused at a high temperature of up to 1600 °C. The released gases were purified successively through activated charcoal traps, and then analyzed for isotopic

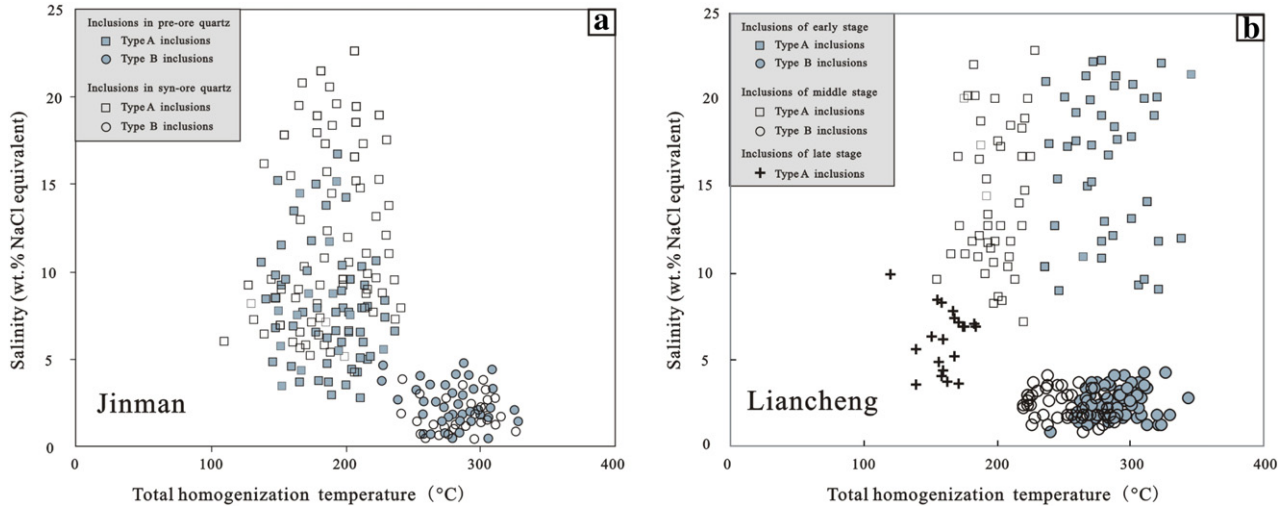

Fig. 10. Plot of homogenisation temperature (T_h) vs. salinity in the ore deposits in the western Lanping basin.

compositions of noble gases on a Micromass UK Limited MM5400 mass spectrometer. The experimental conditions were: It4 = 800 Ma, It40 = 200 μa, 9.000 kv. Additional details of analytical procedures can be found in Ye et al. (2001).

5.2. Analytical results

5.2.1. H and O isotopes

The H and O isotopic compositions of quartz from several representative deposits in the western Lanping basin, obtained in this study, as well as data compiled from previous publications, are presented in Table 3 and Fig. 11 (Gong et al., 2000; Ji and Li, 1998; Li, 2002; Li and Fu, 2000; Li et al., 2005; Liu et al., 2000; Wang, 2010; Xiao, 1989; Zhao, 2006).

On the basis of the oxygen isotope fractionation equation for quartz and water (Zhang, 1985), oxygen isotopic compositions of hydrothermal waters were calculated. Calculations of the fractionation factors were made using the mean homogenization temperatures of fluid inclusions (Table 3). The H-isotopic compositions were measured directly on inclusion fluids. As showed in Table 3, the ore-forming fluids yield more widely variable δD values (−110 to −51‰, mean −89‰), compared with local meteoric water during the Mesozoic–Cenozoic (−90‰ to −110‰, Xu and Mo, 2000). The calculated $\delta^{18}O_{H2O}$ values of the ore-forming fluids vary from −14.8‰ to 9.8‰.

In the δD–δ^{18}O diagram (Fig. 11), the H and O isotopic data from the Cu–Ag (Mo) deposits in the root zone predominately fall between the magmatic (metamorphic) water field and the meteoric line, whereas all the isotopic data from the Pb–Zn–Ag (Cu) deposits plot along the meteoric water line.

5.2.2. C and O isotopes

The C and O isotopic compositions of calcite from Cu–Ag (Mo) deposits in the root zone, obtained by the authors (Zhang, 2013) as well as compiled from previous publications, are presented in Table 4 and Fig. 12 (Liu et al., 2000; Xu and Li, 2003). The δ^{13}C values vary from −7.4 to −1.5‰, and the corresponding δ^{18}O values vary from 13.7‰ to 17.4‰, roughly consistent with the C–O isotopic compositions of limestones in the Lanping basin (Table 4, $\delta^{13}C = -5.5$ to 1.1‰; $\delta^{18}O = 13.7$ to 20.8‰).

5.2.3. He and Ar isotopes

Noble gas isotopic compositions can help discriminate between fluids of mantle, crustal, and meteoric origins. The depleted upper mantle and deep mantle plume-derived fluids yield $^3He/^4He$ ratios of 7 to 9 Ra (Ra = atmospheric ratio, i.e., 1.40×10^{-6}) and 9 to 32 Ra, respectively, which are markedly different from both the atmospheric ratio (1.0) and ratios of shallow crustal hydrothermal fluids (typically in the range of 0.01–0.05 Ra) (Graham et al., 1999; Kendrick et al., 2001, 2006). Moreover, $^{40}Ar/^{36}Ar$ ratios in excess of the atmospheric value of 295.5 may indicate some degree of crustal or mantle component involved in the ore-forming fluids (Bohlke and Irwin, 1992; Mao et al., 2003).

In the Baiyangping Cu–Ag–Pb–Zn ore belt, the lithium concentrations in altered rock and fluid inclusions of the main ore-forming stage are abnormally high (~15 times its abundance in the upper crust, Fan et al., 2006; Wang, 2004). The $^3He/^4He$ ratios may be enriched by the high concentration of lithium, and therefore, noble gas isotopic data from the Baiyangping Cu–Ag–Pb–Zn ore belt are less reliable and should be eliminated (e.g., Fan et al., 2006; Kendrick et al., 2002). Consequently, no data are given for the Baiyangping Cu–Ag–Pb–Zn ore belt.

As show in Table 5, the $^3He/^4He$ ratios of all samples range from 0.01 to 0.07 Ra, all significantly lower than the mantle values, but consistent with typical crustal values (0.01–0.05). The measured $^{40}Ar/^{36}Ar$ values range from 305 to 3034, much greater than the atmospheric value of 295.5, which indicates the presence of a significant proportion of ^{40}Ar of mantle or crustal origin.

Fluid inclusion studies of ore-bearing quartz veins revealed that the trapped fluids were predominantly primary in quartz, which suggested that the extracted fluids in the sulfide minerals were probably related to mineralization. The sulfide minerals analyzed were well-formed euhedral grains, and were collected from underground mines, and so, they provided a very good host for noble gases (Trull et al., 1991). The U, Th, K, and Li contents, from which radiogenic daughter products are produced, are very low in the host minerals and, thus, have almost no influence on the initial isotopic compositions (Norman and Musgrave, 1994; Xue et al., 2007). The atmospheric He contribution can be determined from the F^4He values, defined as the $^4He/^{36}Ar$ ratio of a sample relative to the atmospheric $^4He/^{36}Ar$ value of 0.1655, such that a sample containing air will have an F^4He value of 1 (Kendrick et al., 2001). The F^4He values for inclusion gas from the sulfide minerals from these deposits range from 663 to 64,898 (Table 5), suggesting that contributions of atmospheric He in the fluids are negligible. Therefore, it is believed that the analyzed isotopic compositions represent the original isotopic compositions of ore-forming fluids.

In Fig. 13, all the data are predominately scattered within the crustal-derived (C) field, and far from the mantle-derived (M) field. He and Ar isotopic compositions of fluid inclusions imply that ore-forming fluids of the Cu–Ag–Pb–Zn deposits in the western Lanping basin were

Table 3
Hydrogen and oxygen isotopic compositions of fluid inclusions from the base metal deposits of the western Lanping basin.

Deposit	Sample no.	Mineral	$\delta^{18}O_{min}$ (‰)	T_h (°C)	$\delta^{18}O_{fluid}$ (‰)	δD (‰)	Reference
Jinman	YM-1	Quartz			4.0	−95	Li and Fu (2000)
Jinman	TC-5	Quartz			3.6	−74	
Jinman	LK-5	Quartz			3.6	−99	
Jinman	ZK1505-2	Quartz			4.3	−95	
Jinman	J3-2	Quartz			8.4	−63	Xiao (1989)
Jinman	J3-16	Quartz			3.4	−82	
Jinman	Jinman30-2	Quartz			9.8	−64	
Jinman	JM-1	Quartz			5.4	−51	Ji and Li (1998)
Jinman	JM-18	Quartz			7.3	−101	
Jinman	JM-29	Quartz			5.2	−86	
Jinman	JM-34	Quartz			4.4	−102	
Jinman	LC-3	Quartz			7.0	−95.0	
Jinman	jm-1	Quartz			4.1	−107	Liu et al. (2000)
Jinman	Jinman1-1	Quartz			4.2	−70	Li (2002)
Jinman	Jinman2-1	Quartz			2.2	−72	
Jinman	JM8-6	Quartz			8.0	−90	Wang (2010)
Jinman	JM8-8	Quartz			3.7	−110	
Jinman	JMZD2-2	Quartz			5.0	−104	
Jinman	JMZD2-4	Quartz			5.5	−102	
Jinman	Jm-1	Quartz	17.4	300	9.3	−87	This study
Jinman	Jm-2	Quartz	16.4	300	8.3	−91	
Jinman	Jm-3	Quartz	17.6	300	9.5	−83	
Liancheng	L2-5	Quartz			5.5	−87	Xiao (1989)
Liancheng	v-11	Quartz			6.5	−109	
Liancheng	EN-2	Quartz	17.7	250	7.9	−79	This study
Liancheng	EN-5	Quartz	16.8	280	8.6	−103	
Liancheng	EN-13	Quartz	16.8	250	7.5	−98	
Liancheng	EN-4	Quartz	16.3	280	8.2	−56	
Baiyangping	B-6	Calcite			−14.8	−109	Gong et al. (2000)
Baiyangping	B-10	Calcite			−13.5	−103	
Baiyangping	B-1	Quartz			−10.5	−97	
Baiyangping	HX-24	Calcite			−7.6	−76	Li et al. (2005)
Baiyangping	HX-25-1	Calcite			−7.5	−94	
Baiyangping	HX-26	Calcite			−7.3	−94	
Baiyangping	HX-27	Calcite			−8.4	−93	
Baiyangping	HX-30	Calcite			−8.3	−100	
Baiyangping	By-7	Calcite			−10.4	−87	Zhao (2006)

crust-derived, and the mantle-derived He might be neglected. Excepting for crustal radiogenic Ar, atmospheric Ar was involved in the ore-forming fluids.

5.2.4. S isotopes

The analyzed S isotopic compositions of sulfides, together with those compiled from previous publications (e.g. He et al., 2009; Ji and Li, 1998; Li, 2002; Li and Fu, 2000; Wu et al., 2003; Xiao, 1989; Zhao, 2006), are shown in Table 6 and Fig. 14. The values of sulfides from the Jinman and Liancheng deposits, and from the Baiyanping belt are −17.9‰ to 16.3‰, −10.1 to 12.1‰, and 2.5 to 11.2‰, respectively. Some sulfide minerals that formed in different stages of these deposits may not reach sulfur isotopic equilibrium, especially for the Liancheng Cu–Mo deposit.

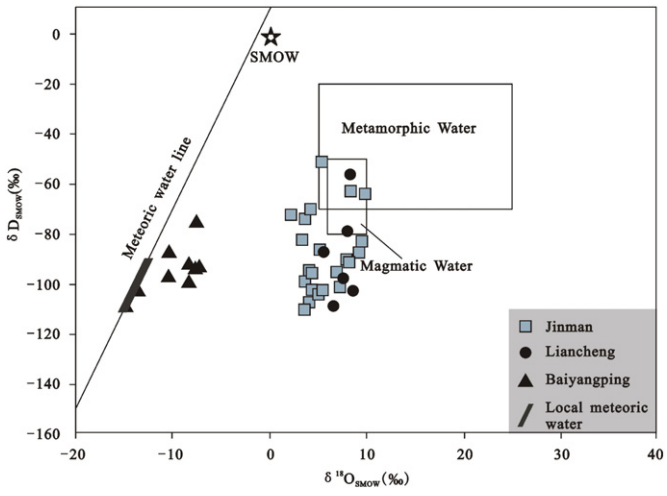

Fig. 11. Measured hydrogen and calculated oxygen isotopic composition of water in ore-forming fluids at the base metal deposits in the western Lanping basin. Local meteoric water values after Xu and Mo (2000).

As shown in Fig. 14, the distribution patterns of $\delta^{34}S$ values differ for each ore belt and deposit. The Jinman deposit yields widely variable $\delta^{34}S$ values, with a tower-shaped distribution around zero. The Liancheng deposit has bimodal $\delta^{34}S$ values (6.1 to 12.1‰ and −10.1 to −1.5; Fig. 14), indicating more than one sulfur source. The Baiyangping ore belt yields a relatively heavy sulfur isotope composition.

5.2.5. Pb isotopes

Pb isotopic compositions for sulfides from the ore deposit and various rocks in the Lanping basin are compiled from previous studies (Li, 2002; Li and Fu, 2000; Wang, 2010; Wu et al., 2003; Zhao, 2006) and presented in Fig. 15.

6. Discussion

6.1. Ore-forming fluids responsible for the Pb–Zn–Cu–Ag mineralization

The Pb–Zn–Cu–Ag deposits in the western Lanping basin record multiple episodes of fluid flow (e.g., Bi and Mo, 2004; He et al., 2004; Li, 2001; Wang et al., 2011; Xue et al., 2003, 2006; Zhang et al., 2013; Zhao, 2006). On the basis of a comprehensive consideration of ore-bearing horizon, ore-controlling structures and isotope chronological data, Zhang et al. (2013) suggested that: (1) the Cu–Ag (Mo) polymetallic mineralization, located in the root zone of the western thrust–nappe system in the

Table 4
C and O isotope data of sulfides from the ore deposit in the western Lanping basin.

Sample no.	Sampling position	Mineral	$\delta^{18}O_{min}$ (‰)	$\delta^{13}C$ (‰)	Reference
JM-4	Jinman	Calcite	13.6	−6.3	This study
JM-3	Jinman	Calcite	16.6	−1.5	
JM-6	Jinman	Calcite	13.7	−4.8	
JM-3	Jinman	Calcite	14.6	−3.9	
JM-11	Jinman	Calcite	14.6	−4.1	
JMC-1	Jinman	Calcite	15.6	−5.9	
JMC-4	Jinman	Calcite	14.8	−5.8	
JMD-11	Jinman	Calcite	14.0	−5.2	
09JM-10	Jinman	Calcite	14.4	−6.5	
S01134	Jinman	Calcite	15.5	−6.6	Xu and Li (2003)
y-12	Jinman	Calcite	16.6	−7.4	Liu et al. (2000)
09EN-5	Liancheng	Calcite	17.4	−4.1	This study
09EN-4	Liancheng	Calcite	16.4	−5.6	
09EN-12	Liancheng	Calcite	15.4	−4.8	
LC02-3	Liancheng	Calcite	15.4	−5.1	
LC02-5	Liancheng	Calcite	15.7	−4.7	
LCD-5	Liancheng	Calcite	15.6	−5.0	
LP08-23	Liancheng	Calcite	16.1	−6.6	
LC014-7	Liancheng	Calcite	15.7	−6.2	
Strata and rocks					
Upper Triassic Limestone			15.3	0.6	Xu and Li (2003)
Upper Triassic Limestone			13.7	−0.8	
Upper Triassic Limestone			15.0	1.1	
Upper Triassic Limestone			20.8	−5.5	
Upper Triassic Limestone			17.6	−2.1	This study
Middle Jurassic Limestone			20.4	−1.7	

western Lanping basin, mainly took place at ca. 56–48 Ma, corresponding to the main collisional stages of the Indo-Asian orogeny; and (2) the mineralization ages of Pb–Zn–Ag (Mo) deposits located in the front zone were likely to be ca. 30–28 Ma, corresponding to the late-collisional stages of the Indo-Asian orogeny.

Fluid inclusion and stable isotopic data, combined with $^{40}Ar/^{39}Ar$, K–Ar, Re–Os, and Sm–Nd ages (e.g., Bi and Mo, 2004; He et al., 2004; Li, 2001; Wang et al., 2011; Xue et al., 2003, 2006; Zhang et al., 2013; Zhao, 2006), reveal that there were at least two distinct fluid systems operating in the western Lanping basin. The properties of mineralizing fluids in the Cu–Ag (Mo) and Pb–Zn–Ag (Cu) polymetallic deposits are discussed in more detail below.

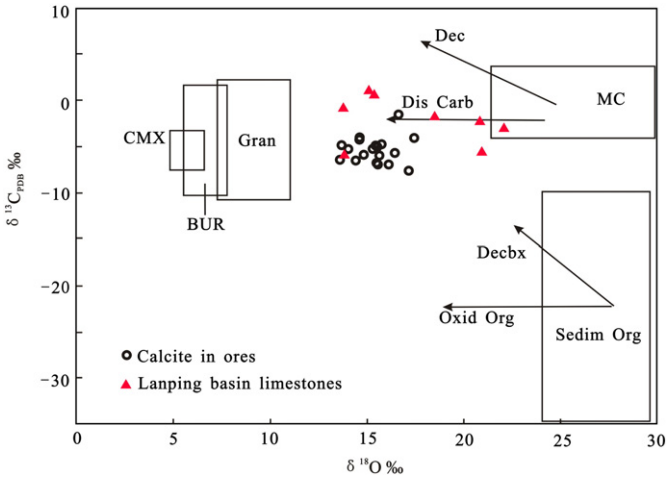

Fig. 12. Carbon and oxygen isotopic composition of calcite in ores from the vein copper deposits and unaltered limestones in the Lanping basin (after Xu and Li (2003)). For reference, the fields for typical marine carbonates (MC), sedimentary organic matter (Sedim Org), and igneous carbonate (CMX carbonatite and mantle xenoliths; BUR basic and ultrabasic rocks; Gran granite) are outlined. The arrows show typical isotopic trends resulting from carbonate dissolution (Dis Carb), decarbonation (Dec), decarboxylation of organic matter (Decbx), and oxidation of organic matter (Oxid Org).

6.2. Ore-forming fluids for the Pb–Zn–Ag (Cu) mineralization in the front zone

Ore-forming fluids responsible for the Pb–Zn–Ag (Cu) deposits in the front zone are characterized by aqueous inclusions, with few CO_2-bearing inclusions (Xu et al., 2005; Xue et al., 2010). The ore-forming fluids of the Baiyangping Cu–Ag–Pb–Zn ore belt have low temperatures and moderate to medium–high salinities, similar to fluids from MVT and SEDEX deposits (He et al., 2009; Xue et al., 2010). Xu and Zhou (2004), Xue et al. (2006, 2007), and He et al. (2009) proposed that regional basinal brines were widely developed, with relatively low temperature and high salinity, in the Lanping basin. Therefore, these authors suggested basinal brines were the main source of ore-forming fluids responsible for Pb–Zn–Ag (Cu) mineralization in the front zone. This is supported by H and O isotopic compositions of fluids, which have the least exchanged meteoric water signature.

Compared with typical basinal brines, some fluid inclusions in the Pb–Zn–Ag (Cu) deposits yield lower salinities (<10 wt.% NaCl equivalent), which can be interpreted as the result of fluid mixing of meteoric water and basinal brine.

6.3. Ore-forming fluids for the Cu–Ag (Mo) mineralization in the root zone

Ore-forming fluids responsible for Cu–Ag (Mo) mineralization in the root zone are characterized by CO_2-bearing inclusions and aqueous inclusions. The CO_2-bearing inclusions are marked by relatively high temperatures and low salinities, whereas the aqueous inclusions show relatively low to medium–high temperatures and medium–high salinities (Figs. 9, 10). The ore-forming fluids responsible for Cu–Ag mineralization in the root zone have systematically higher temperatures than those associated with the Pb–Zn–Ag (±Cu) deposits in the front zone. This is uncharacteristic of basinal fluid systems, but comparable to those of orogenic or magmatic hydrothermal systems (Cameron and Hattori, 1987; Chen et al., 2007; Chi and Xue, 2011; Diamond, 2001; Phillips and Powell, 1993; Rosenbaum et al., 1996; Wilkinson, 2001). Additionally, at the Jinman and Liancheng deposits, CO_2-bearing inclusions commonly coexist with aqueous inclusions in groups or along

Table 5
He and Ar isotope data of sulfides from the ore deposit in the western Lanping basin.

Sample no.	Deposits	Minerals	$^4He(\times10^{-7})$	$^3He/^4He$ (Ra)	$^{40}Ar(\times10^{-7})$	$^{40}Ar/^{36}Ar$	F^4He
09JM-14	Jinman–Liancheng	Chalcopyrite	1.37 ± 0.10	0.06	3.81 ± 0.27	305	663
JMC-17	Jinman–Liancheng	Chalcopyrite	0.59 ± 0.05	0.01	1.03 ± 0.07	1142	3961
JMD-5	Jinman–Liancheng	Chalcopyrite	3.03 ± 0.21	0.02	4.83 ± 0.33	561	2126
EQ-20	Jinman–Liancheng	Chalcopyrite	2.25 ± 0.16	0.04	2.81 ± 0.20	333	1631
En-6	Jinman–Liancheng	Chalcopyrite	3.52 ± 0.24	0.07	2.64 ± 0.19	322	2596
LC02-1	Jinman–Liancheng	Pyrite	1.31 ± 0.10	0.02	1.64 ± 0.12	852	4116
EQ-2	Jinman–Liancheng	Chalcopyrite	37.9 ± 2.5	0.01	0.80 ± 0.06	438	12,924
hb-25	Kedengjian	Chalcopyrite	136.7 ± 9.2	0.03	27 ± 2.2	911	27,878
hb-15	Kedengjian	Bornite	3.82 ± 0.26	0.05	1.08 ± 0.08	3034	64,898

the same trail, which is interpreted as evidence for fluid immiscibility (Chi and Xue, 2011; Lu et al., 2004; Roedder, 1984).

In the case of the Liancheng Cu–Mo deposit, the interpretation of fluid immiscibility is further supported by the distribution pattern of homogenization temperatures and salinities (Figs. 9, 10). The type B inclusions in quartz of the early ore forming stage yield homogenization temperatures of 343–240 °C, indistinguishable from associated aqueous inclusions (346–236 °C). Furthermore, the quartz–sulfide stages of the Liancheng Cu–Mo deposits are characterized by bimodal salinity values (Figs. 9, 10), indicating the presence of two co-existing ore forming fluids or phases (Anderson et al., 1992; Lu et al., 2004; Mao et al., 2003; Roedder, 1992). In addition to fluid immiscibility, fluid mixing probably occurred in the Liancheng Cu–Mo deposit, as suggested by the different homogenization temperatures of Type A and Type B fluid inclusions in the middle stage. Moreover, the wide distribution of $\delta^{34}S$ values also supports this interpretation.

However, this phenomenon is difficult to interpret as the result of fluid immiscibility in the case of the Jinman deposit, because type A inclusions in both pre- and syn-ore quartz yield significantly lower homogenization temperatures (160–250 °C) than type B inclusions (226–334 °C). Furthermore, in the salinity–total homogenization temperature diagram (Fig. 10), a slight negative correlation was observed between homogenization temperature and corresponding salinity, especially for data from different types of fluid inclusions. This phenomenon is generally interpreted as evidence for mixing of CO_2-rich fluids and aqueous-rich fluids (Chi and Xue, 2011; Lu et al., 2004). In view of the fact that regional basinal brines are widely developed in the Lanping basin, the aqueous inclusions in both pre- and syn-ore quartz from the Jinman deposit represent basinal fluid unrelated to the CO_2-rich fluids (Chi and Xue, 2011).

There are four possible sources proposed in the literature for the CO_2-bearing inclusions: magmatic origin, metamorphic origin, mantle origin, or carbonate dissolution (Cameron and Hattori, 1987; Chen et al., 2007; Diamond, 2001; Higgins and Kerrich, 1982; Kerrich and Fyfe, 1981; Phillips and Powell, 1993; Rosenbaum et al., 1996; Su et al., 2009; Wilkinson, 2001).

Fig. 12 shows that the carbon and oxygen isotopic compositions of hydrothermal calcite in the ores from several Cu–Ag (Mo) deposits in the root zone are similar to those of the limestones in the Lanping basin. Although the lower $\delta^{13}C$ values also permit a magmatic origin, the lack of coeval intrusions near most deposits discounts this possibility. Therefore, the higher CO_2 content of the CO_2-rich fluid in the Cu–Ag (Mo) deposits is interpreted as resulting from carbonate dissolution at the level of the deposits. Fig. 11 shows the H and O isotopic composition of water in ore fluids and the local meteoric water during the Mesozoic–Cenozoic. The δD values of water in ore fluids are approximately equivalent to those of meteoric water, but the $\delta^{18}O_{H2O}$ values are much greater. The positive shift of $\delta^{18}O_{H2O}$ values toward those of the sedimentary host rocks suggests the ore fluids consisted of meteoric water that evolved via isotopic exchange with country rocks at elevated temperatures. Also, the H and O isotopic compositions can be interpretation by the mixing of meteoric and magmatic or/and metamorphic waters, because some isotopic data in Fig. 11 plot close to, and below the fields for magmatic and metamorphic water. Therefore, we suggest that magmatic or/and metamorphic fluids may be involved in the mineralization, although the causative intrusions and coeval metamorphism cannot be identified.

There is no evidence for mantle fluid involvement, because noble gas isotope compositions reveal that the ore-forming fluids in the Cu–Ag (Mo) deposits show features of crustal-derived fluid, without a mantle component (Fig. 13). Deep magmatic and metamorphic components seem to be another likely fluid source for the CO_2-rich fluid, although the lack of coeval igneous and metamorphic rocks in the vicinity of the deposits discounts this possibility.

As stated above, Cu–Ag (Mo) mineralization in the root zone is dominated by deeply circulating meteoric water, but we do not exclude the possibility of participation of magmatic or metamorphic components. In comparison, hydrothermal activity associated with the Pb–Zn–Ag (±Cu) deposits in the front zone is characterized by basinal brine, which is marked by low temperatures (130 °C to 180 °C), high salinities (9 to 24 wt.% NaCl equivalent), and low in CO_2.

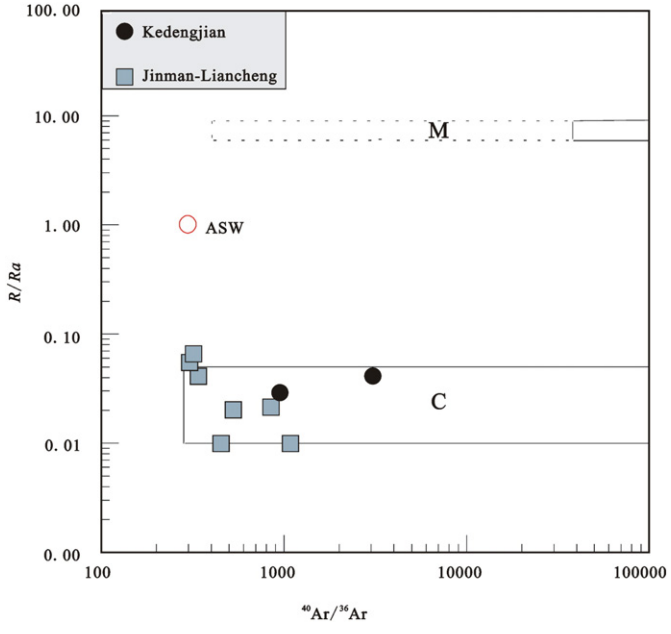

Fig. 13. $^{40}Ar/^{36}Ar$–R/Ra diagram of the base metal deposits in the western Lanping basin. ASW—air saturated water; M—mantle-derived fluids; C—crustal fluids (after Mao et al. (2003)).

6.4. Source of the ore-forming materials

The base metal deposits in the western Lanping basin show wide variations in sulfide $\delta^{34}S$ values (Fig. 14), −17.9 to 16.3‰ for the Cu–Ag

Table 6
S isotope data of sulfides from the ore deposit in the western Lanping basin.

Sample no.	Mineral	$\delta^{34}S$(CDT) ‰	Sample no.	Mineral	$\delta^{34}S$(CDT) ‰
Jinman					
After Ji and Li (1998)			After Zhao (2006)		
JM-1	Tetrahedrite	7.99	JM3-2	Chalcocite	−7.60
JM-3	Chalcopyrite	−0.51	JM3-2	Bornite	−7.20
JM-6	Chalcopyrite	−1.57	JM3-6	Chalcopyrite	−4.80
JM-9	Bornite	−9.32	JM3-12	Chalcopyrite	−7.20
JM-10	Chalcopyrite	−8.86	data obtained in this study		
JM-15	Chalcopyrite	−0.52	JMC-20	Chalcocite	−5.66
JM-19	Pyrite	−5.83	09JM-8	Chalcocite	4.08
JM-35	Bornite	−2.47	JMC-3	Chalcocite	−5.46
After Xiao (1989)			JMC-13-3	Tetrahedrite	−8.55
Jiangxi-1	Tetrahedrite	−4.57	JM-4	Chalcopyrite	4.06
Jiangxi-2	Bornite	−5.49	JM-14	Tetrahedrite	16.26
Jiangxi-3	Chalcopyrite	−5.86	JM-14-1	Tetrahedrite	10.82
Jiangdong-1	Tetrahedrite	−0.08	JMC-14	Bornite	−6.74
Jiangdong-2	Bornite	−9.63	JMC-16	Bornite	−17.94
Jiangdong-3	Chalcopyrite	−1.34	JMC-18	Bornite	−10.31
After Li (2002)			JMC-20	Bornite	−7.50
Jinman1-1	Chalcocite	−2.80	JM-13	Chalcopyrite	−1.76
Jinman1-1	Pyrite	−2.30	JMC-8	Chalcopyrite	5.53
Jinman2-1	Pyrite	−4.40	JMC-10	Chalcopyrite	−1.34
After Wu et al. (2003)			JMC-16	Chalcopyrite	−2.21
JM-4	Chalcopyrite	−10.20	JMC-17	Chalcopyrite	0.68
JM-4	Tetrahedrite	3.20	09JM-14	Chalcopyrite	−2.15
JM-12	Tetrahedrite	1.10	JMD-3	Chalcopyrite	3.78
JM-23	Chalcopyrite	−15.50	09JM-20	Chalcopyrite	−10.61
Liancheng (all data obtained in this study)					
EN-3	Chalcopyrite	−9.10	LCD-5	Bornite	−7.88
EN-4	Chalcopyrite	−8.97	09EN-19	Bornite	−9.57
EN-5	Chalcopyrite	−3.20	EN-1	Molybdenite	−8.29
EN-6	Chalcopyrite	−3.19	EN-2	Molybdenite	−8.30
EN-7	Chalcopyrite	−7.90	EN-3	Molybdenite	−7.84
EN-8	Chalcopyrite	−6.23	EN-4	Molybdenite	−6.56
EN-12	Chalcopyrite	−5.58	09EN-3	Molybdenite	−8.63
EN-13	Chalcopyrite	−5.42	LC02-1	Molybdenite	−8.64
09EN-13-1	Chalcopyrite	−1.45	LC03-4	Molybdenite	−7.87
LCD-1	Chalcopyrite	−3.63	LC03-7	Molybdenite	−8.24
LC02-1	Chalcopyrite	−4.64	LC03-8	Molybdenite	−7.72
LC02-7	Chalcopyrite	−7.07	LC03-9	Molybdenite	−5.82
LC03-2	Chalcopyrite	−5.21	En-3-2	Tetrahedrite	−7.41
LC03-6	Chalcopyrite	6.05	EN-4-2	Tetrahedrite	−8.93
LC03-10	Chalcopyrite	−8.70	EN-5-2	Tetrahedrite	−7.40
LC02-7-5	Pyrite	−4.09	EN-7-2	Tetrahedrite	−7.64
LC02-1	Pyrite	−10.05	EN-8-2	Tetrahedrite	−8.60
LC02-2	Chalcocite	−2.26	EN-13-2	Tetrahedrite	−4.49
LCD-5	Chalcocite	−4.52	En-14	Tetrahedrite	−5.70
09EN-5	Chalcocite	−3.85	En-13	Tetrahedrite	−6.10
LC03-2	Bornite	−3.54	En-16	Tetrahedrite	−5.90
LC03-5-2	Bornite	10.87	En-19	Tetrahedrite	−4.90
LC03-6	Bornite	12.11			
Baiyangping					
After Wei (2001)			After Li et al. (2005)		
B-1	Chalcopyrite	2.51	FLC-147	Tetrahedrite	9.20
B-2	Tetrahedrite	6.10	FLC161	Tetrahedrite	7.90
B-3	Bornite	5.84	FLC149	Sphalerite	10.50
F-1	Galena	2.54	FLC-160	Sphalerite	10.00
F-2	Galena	5.03	FLC-176	Sphalerite	11.20
After Wang and He (2003)			BY-3-1	Tetrahedrite	5.80
B4-2	Tetrahedrite	6.71	BY-3-2	Tetrahedrite	9.30
B4-3	Tetrahedrite	6.79	H-1	Tetrahedrite	3.50
B4-4	Tetrahedrite	6.91	H-2	Tetrahedrite	4.80

(Mo) deposits, and 2.5 to 11.2‰ for Pb–Zn–Ag (±Cu) deposits, respectively. This variation may be interpreted as resulting from the variations in physicochemical conditions or from compositional variations of the sources.

The predominance of positive $\delta^{34}S$ values (mean = 6.7‰) of sulfides in the Pb–Zn–Ag (Cu) deposits in the front zone indicate that the reduced S was mainly derived from reduction of sulfates in the basin strata (He et al., 2009; Wu et al., 2003). This interpretation is supported by the widely distributed evaporite sulfates in the Lanping basin, which yield relatively positive $\delta^{34}S$ values.

In contrast, the origin of reduced S for the Cu–Ag (Mo) deposits in the root zone is more controversial. As for the sulfur source for the Jinman deposit, there have been different interpretations proposed by previous researchers. On the basis of the widely variable $\delta^{34}S$ values of sulfides in the Jinman deposit, Xiao et al. (1994), Liu et al. (2000), and Wu et al. (2003) proposed that the reduced S was mainly derived

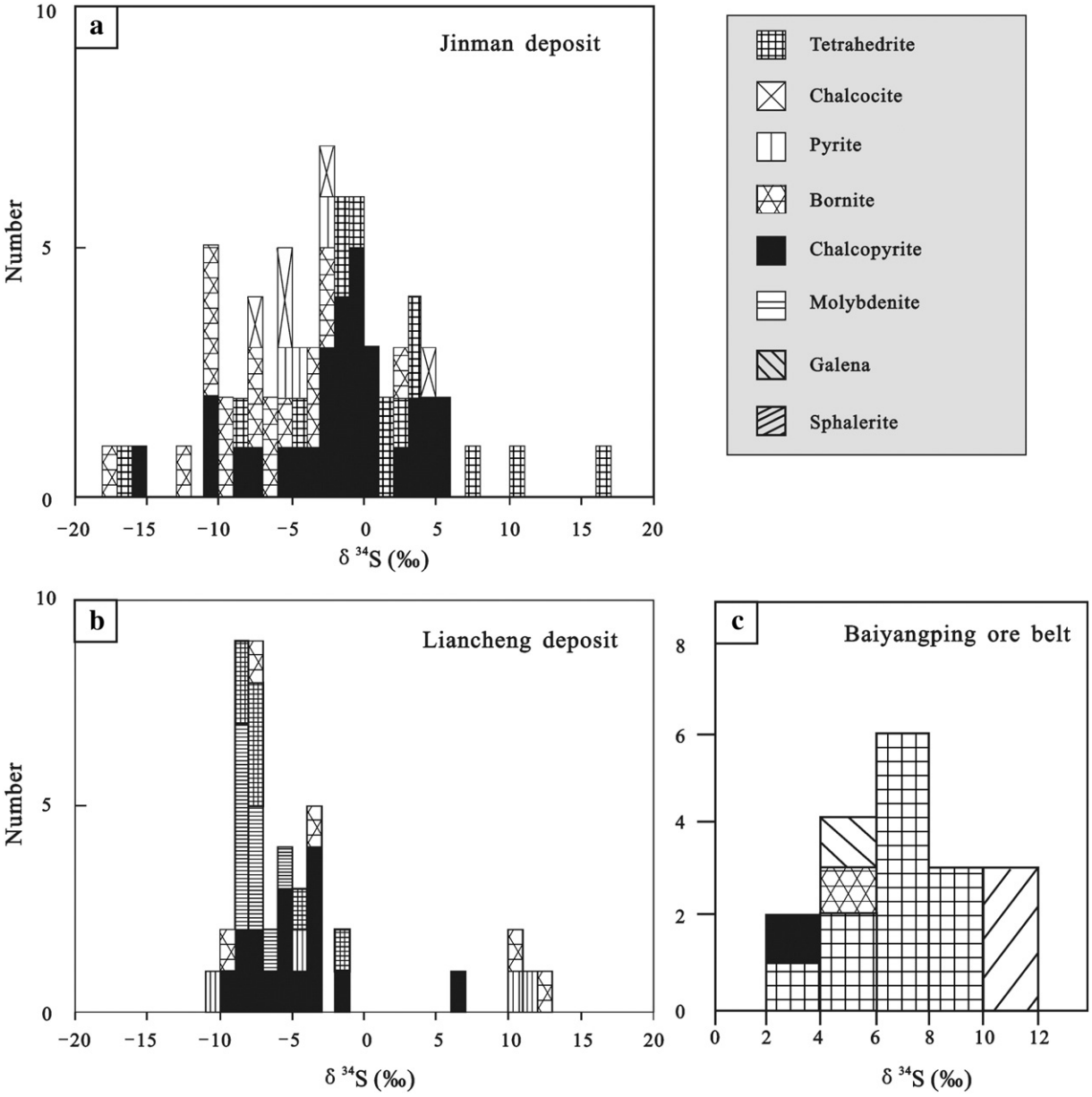

Fig. 14. Histogram of sulfur isotopic compositions of sulfides from the ore deposit in the western Lanping basin.

from the basin strata, including extraction from organic matter and the reduction of sulfates. However, the clustering of $\delta^{34}S$ values around zero in the Jinman deposit revealed that the reduced S might derive from a deep source (Ji and Li, 1998; Yan and Li, 1997). Ohmoto and Rye (1979) proposed that the widely variable $\delta^{34}S$ values of the sulfides could be interpreted as resulting from variations in physical–chemical conditions of the ore-forming fluids or diverse sources of the sulfur. On the basis of synthetic analysis, we suggest that the reduced S for sulfide precipitation in the Jinman deposit may mainly originate from sedimentary rocks in the basin, but we do not exclude the possibility of participation of sulfur from deep-crustal magma. The bimodal $\delta^{34}S$ values (6.1–12.1‰ and −10.1 to −1.5‰; Fig. 14) of the sulfides from the Liancheng deposit also indicate the presence of multiple sulfur sources. The lead isotopic compositions of sulfides are consistent with the crustal lead isotopic compositions in the Lanping–Simao basin, but significantly different from the upper mantle lead in the Lanping Basin, as derived from the study of mantle enclaves in Cenozoic magmatic intrusions (Xue et al., 2007; Zhang et al., 2002). Moreover, Pb isotopes of the ore belt/deposits are closer to the sedimentary rocks in the Lanping basin (Fig. 15), which indicates that the metallogenic materials, at least ore lead, are predominantly derived from the crustal rocks in the Lanping basin.

7. Conclusions

A series of thrust-controlled sediment-hosted Himalayan Cu–Ag–Pb–Zn polymetallic deposits have been discovered in the western Lanping basin, on the eastern margin of the Tibetan Plateau, southwestern China. These deposits are mainly hosted in Mesozoic–Cenozoic mottled clastic rocks, and controlled by Cenozoic thrust systems related to Indo-Asian collision since the Paleocene. In the thrust–nappe system, Cu–Ag (Mo) deposits mainly occur in the root zone, whereas Pb–Zn–Ag (Cu) deposits mainly occur in the front zone.

Fluid inclusion studies reveal that the ore-forming fluids responsible for the vein-type Cu–Ag (Mo) deposits are characterized by

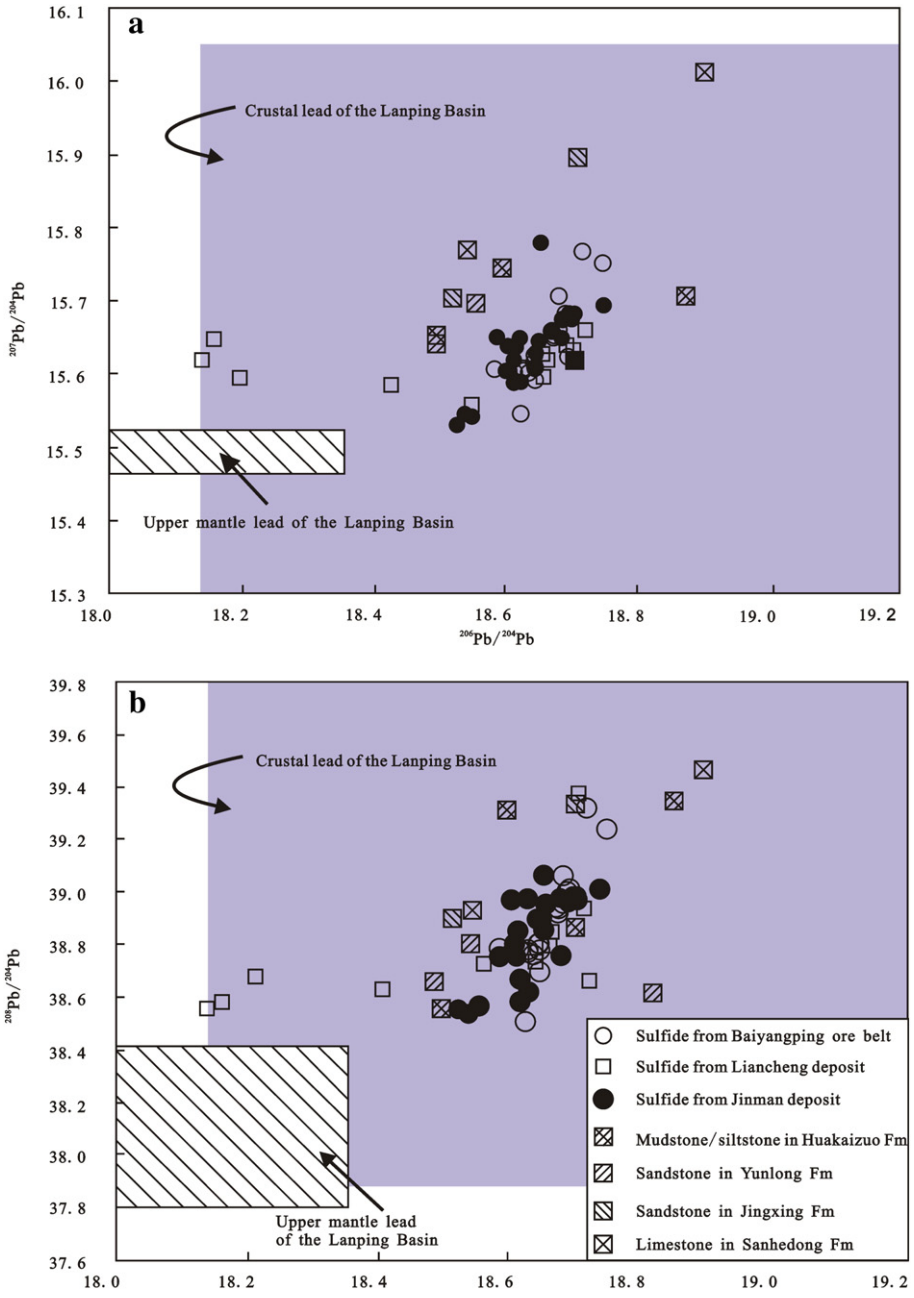

Fig. 15. Histogram of Pb isotopic compositions of sulfides from the ore deposits in the western Lanping basin.

abundant CO_2-rich fluid inclusions, which are significantly different from the basinal fluids that formed the Pb–Zn deposits in other parts of the Lanping Basin. Carbon–oxygen isotopic studies reveal that CO_2 in the CO_2-rich fluids of the Cu–Ag (Mo) deposits results from carbonate dissolution.

After comprehensive analyses of the geology, fluid inclusions, and C, H, O, He, and Ar isotopic geochemistry of the Cu–Ag (Mo) deposits and Pb–Zn–Ag (Cu) deposits in the western Lanping basin, we suggest that the Cu–Ag (Mo) mineralization in the root zone is dominated by deeply circulating meteoric water. Magmatic or metamorphic fluid components probably are involved in the mineralization. In contrast, hydrothermal activity associated with the Pb–Zn–Ag (Cu) deposits in the front zone is characterized by basinal brines. Sulfur and Pb isotopic compositions indicate that the ore-forming metals are predominantly derived from sedimentary rocks in the basin.

Acknowledgments

This work was financially supported by, the National Natural Science Foundation for the Youth (no. 41403038), the 12th Five-Year Plan project of the State Key Laboratory of Ore-deposit Geochemistry, the National Natural Science Foundation of China (grant nos. 40930425, 41173026), and the Comprehensive Research Project of China Geological Survey (12120113094400). We are grateful to the geological workers from the Sanjiang Copper Company Limited for their assistance during our field investigation.

References

Anderson, M.R., Rankin, A.H., Spiro, B., 1992. Fluid mixing in the generation of mesothermal gold mineralization in the Transvaal sequence, Transvaal, South Africa. Eur. J. Mineral. 5, 933–948.

Bi, X.M., Mo, X.X., 2004. Transition from diagenesis to low-grade metamorphism and related minerals and energy resources. Earth Sci. Front. 11, 287–294 (in Chinese with English abstract).

Bodnar, R.J., 1993. Revised equation and table for determining the freezing point depression of H_2O–NaCl solutions. Geochim. Cosmochim. Acta 57, 683–684.

Bohlke, J.K., Irwin, J.J., 1992. Laser microprobe analyses of noble gas isotopes and halogens in fluid inclusions: analyses of microstandards and synthetic inclusions in quartz. Geochim. Cosmochim. Acta 56, 187–201.

Cameron, E.M., Hattori, K., 1987. Archean gold mineralization and oxidized hydrothermal fluids. Econ. Geol. 82, 1177–1191.

Chen, K.X., He, L.Q., Yang, Z.Q., Wei, J.Q., Yang, A.P., 2000. Oxygen and carbon isotope geochemistry in Sanshan–Baiyangping copper–silver polymetallogenic enrichment district, Lanping, Yunnan. Geol. Miner. Resour. South China 4, 1–8 (in Chinese with English abstract).

Chen, Y.J., Ni, P., Fan, H.R., Pirajno, F., Lai, Y., Su, W.C., Zhang, H., 2007. Diagnostic fluid inclusions of different types of hydrothermal gold deposits. Acta Petrol. Sin. 23, 2085–2108 (in Chinese with English abstract).

Chi, G.X., Xue, C.J., 2011. Abundance of CO_2-rich fluid inclusions in a sedimentary basin-hosted Cu deposit at Jinman, Yunnan, China: implications for mineralization environment and classification of the deposit. Mineral. Deposita 46, 365–380.

Diamond, L.W., 2001. Review of the systematics of CO_2–H_2O fluid inclusions. Lithos 55, 69–99.

Dong, F.L., Mo, X.X., Hou, Z.Q., Wang, Y., Bi, X.M., Zhou, S., 2005. $^{40}Ar/^{39}Ar$ ages of Himalayan alkaline rocks in the Lanping basin, Yunnan and their geological significance. Acta Petrol. Mineral. 24, 103–109 (in Chinese with English abstract).

Fan, S.J., Wang, A.J., Liu, H.B., Xiu, Q.Y., Chao, D.H., Li, R.P., Gao, H., Chen, Q.S., 2006. A discussion on the Helium and Argon isotopic evidences for genesis of the Baiyangping Copper–Cobalt deposit in the Lanping Basin. Geol. Rev. 52, 628–635 (in Chinese with English abstract).

Gong, W.J., Tan, K.X., Li, X.M., Gong, G.L., 2000. Geochemical characteristics of fluid and mechanism for ore formation in the Baiyangping copper–silver deposit, Yunnan. Geotecton. Metallog. 24, 175–181 (in Chinese with English abstract).

Graham, D.W., Johnson, K.T.M., Douglas, P.L., Lupton, J.E., 1999. Hotspot–ridge interaction along the Southeast Indian Ridge near Amsterdam and St. Paul islands: helium isotope evidence. Earth Planet. Sci. Lett. 167, 297–310.

He, M.Q., Liu, J.J., Li, C.Y., Li, Z.M., Liu, Y.P., 2004. Mechanism of Ore–forming Fluids of the Lanping Pb–Zn–Cu Polymetallic Mineralized Concentration Area—An Example Study on the Baiyangping Ore District. Geological Publishing House, Beijing, pp. 1–108 (in Chinese with English abstract).

He, L.Q., Song, Y.C., Chen, K.X., Hou, Z.Q., Yu, F.M., Yang, Z.S., Wei, J.Q., Li, Z., Liu, Y.C., 2009. Thrust-controlled, sediment-hosted, Himalayan Zn–Pb–Cu–Ag deposits in the Lanping foreland fold belt, eastern margin of Tibetan Plateau. Ore Geol. Rev. 36, 106–132.

Higgins, N.C., Kerrich, R., 1982. Progressive ^{18}O depletion during CO_2 separation from a carbon-dioxide-rich hydrothermal fluid: evidence from the Grey River tungsten deposit, Newfoundland. Can. J. Earth Sci. 19, 2247–2257.

Hou, Z.Q., Pan, G.T., Wang, A.J., Mo, X.X., Tian, S.H., Sun, X.M., Ding, L., Wang, E.Q., Gao, Y.F., Xie, Y.L., Zeng, P.S., Qin, K.Z., Xu, J.F., Qu, X.M., Yang, Z.M., Yang, Z.S., Fei, H.C., Meng, X.J., Li, Z.Q., 2006. Metallogenesis in Tibetan collisional orogenic belt: II. Mineralization in late-collisional transformation setting. Mineral Deposits 25, 521–543 (in Chinese with English abstract).

Hou, Z.Q., Khin, Z., Pan, G.T., Mo, X.X., Xu, Q., Hu, Y.Z., Li, X.Z., 2007. Sanjiang Tethyan metallogenesis in S.W. China: tectonic setting, metallogenic epochs and deposit types. Ore Geol. Rev. 31, 48–87.

Hou, Z.Q., Song, Y.C., Li, Z., Wang, Z.L., Yang, Z.M., Yang, Z.S., Liu, Y.C., Tian, S.H., He, L.Q., Chen, K.X., Wang, F.C., Zhao, C.X., Xue, W.W., Lu, H.F., 2008. Thrust-controlled, sediments-hosted Pb–Zn–Ag–Cu deposits in eastern and northern margins of Tibetan orogenic belt: geological features and tectonic model. Mineral Deposits 27, 123–144 (in Chinese with English abstract).

Ji, H.B., Li, C.Y., 1998. Geochemical characteristics and source of ore-forming fluid for Jinman copper deposit in western Yunnan Province, China. Acta Mineral. Sin. 18, 28–37 (in Chinese with English abstract).

Kendrick, M.A., Burgess, R., Pattrick, R.A.D., Turner, G., 2001. Fluid inclusion noble gas and halogen evidence on the origin of Cu-porphyry mineralizing fluids. Geochim. Cosmochim. Acta 65, 2651–2668.

Kendrick, M.A., Burgess, R., Leach, D., Pattrick, R.A., 2002. Hydrothermal fluid origins in Mississippi valley-type ore districts: combined noble gas (He, Ar, Kr) and halogen (Cl, Br, I) analysis of fluid inclusions from the Illinois–Kentucky Fluorspar District, Viburnum Trend, and Tri-State Districts, Midcontinent United States. Econ. Geol. 97, 453–469.

Kendrick, M.A., Duncan, R., Phillips, D., 2006. Noble gas and halogen constraints on mineralizing fluids of metamorphic versus surficial origin: Mt Isa, Australia. Chem. Geol. 235, 325–351.

Kerrich, R., Fyfe, W.S., 1981. The gold–carbonate associations: source of CO_2 and CO_2 fixation reactions in Archean lode deposits. Chem. Geol. 33, 265–294.

Khin, Z., Peters, S.G., Gromie, P., Burrett, C., Hou, Z.Q., 2007. Nature, diversity of deposit types and metallogenic relations of South China. Ore Geol. Rev. 31, 3–47.

Kong, Y.L., Qi, L.K., 2009. The genesis of Liziping Pb–Zn deposit of Zhongpai in Lanping, Yunnan (in Chinese). Yunnan Geol. 28, 275–279.

Kyle, J.K., Li, N., 2002. Jinding: a giant Tertiary sandstone-hosted Zn–Pb deposit, Yunnan, China. SEG. Newslett. 50, 8–16.

Li, X.M., 2001. Metallogenic age of Jinman copper deposits in western Yunnan Province, China. Geoscience 15, 405–408 (in Chinese with English abstract).

Li, Y.S., 2002. The geochemical studies on copper polymetallic deposits of middle-southern part of Lanchangjiang, Yunnan Province, China. (Master Report), Hefei University of Technology, Hefei (74 pp. (in Chinese with English abstract)).

Li, F., Fu, W.M., 2000. Geology of Red Bed Copper Deposits in Western Yunnan. Yunnan University Press, Kunming, p. 133 (in Chinese with English abstract).

Li, Z.M., Liu, J.J., Qin, J.Z., Liao, Z.T., He, M.Q., Liu, Y.P., 2005. Ore-forming material source of the Baiyangping copper–cobalt–silver polymetallic deposit in Lanping basin, Western Yunnan. Geol. Prospect. 1, 1–6 (in Chinese with English abstract).

Liu, J.J., Li, C.Y., Pan, J.Y., Liu, X.F., Liu, Y.P., 2000. Metallogenic mechanism of copper deposits from sandstone to shale in Lanping–Simao basin, western Yunnan. Geol. Miner. Resour. Res. 15, 216–223 (in Chinese with English abstract).

Liu, J.J., Li, C.Y., Zhang, Q., Pan, J.Y., Liu, Y.P., Liu, X.F., Liu, S.R., Yang, W.G., 2001. Wood textures in the Jinman Cu deposit in western Yunnan and their significance for ore genesis. Sci. China Ser. D 31, 89–95 (in Chinese with English abstract).

Lu, H.Z., Fan, H.R., Ni, P., Ou, G.X., Shen, K., Zhang, W.H., 2004. Fuild Inclusions. Science Press, Beijing, p. 487 (in Chinese with English abstract).

Luo, J.L., Yang, J.Z., 1994. The Tethyan Evolution and the Mineralization of the Main Metal Deposits in Western Yunnan. Geological Publishing House, Beijing, pp. 149–239 (in Chinese with English abstract).

Mao, J.W., Li, Y.Q., Goldfarb, R.J., He, Y., Zaw, K., 2003. Fluid inclusion and noble gas studies of the Dongping gold deposit, Hebei province, China: a mantle connection for mineralization? Econ. Geol. 98, 517–534.

Mu, C.L., Wang, J., Yu, Q., Zhang, L.S., 1999. The evolution of the sedimentary basin in Lanping area during Mesozoic–Cenozoic. Miner. Petrol. 19, 30–36 (in Chinese with English abstract).

Norman, D.I., Musgrave, J.A., 1994. N_2–He–Ar compositions in fluid inclusions: indicators of fluid source. Geochim. Cosmochim. Acta 58, 1119–1132.

Ohmoto, H., Rye, R.O., 1979. Isotopes of sulfur and carbon. In: Barnes, H.L. (Ed.), Geochemistry of Hydrothermal Ore Deposits. Wiley, New York, pp. 509–567.

Phillips, G.N., Powell, J.K., 1993. Link between gold provinces. Econ. Geol. 88, 1084–1098.

Qin, G.J., Zhu, S.Q., 1991. The ore-forming model of the Jinding lead–zinc deposit and prediction. J. Yunnan Geol. 10, 145–190 (in Chinese with English abstract).

Que, M.Y., Cheng, D.M., Zhang, L.S., Xia, W.J., Zhu, C.Y., 1998. Copper Deposits in Lanping–Simao Basin. Geological Publishing House, Beijing, pp. 59–109 (in Chinese with English abstract).

Roedder, E., 1984. Fluid inclusions. Rev. Mineral. 12 (644 pp.).

Roedder, E., 1992. Fluid inclusion evidence for immiscibility in magmatic differentiation. Geochim. Cosmochim. Acta 56, 5–20.

Rosenbaum, J.M., Zindler, A., Rubenstone, J.L., 1996. Mantle fluids: evidence from fluid inclusions. Geochim. Cosmochim. Acta 60, 3229–3252.

Shi, J.X., Yi, F.H., Wen, Q.D., 1983. The rock-ore characteristics and mineralisation of Jinding lead–zinc deposit, Lanping. J. Yunnan Geol. 2, 179–195 (in Chinese with English abstract).

Song, Y.C., Hou, Z.Q., Yang, T.N., Zhang, H.R., Yang, Z.S., Tian, S.H., Liu, Y.C., Wang, X.H., Liu, Y.X., Xue, C.D., Wang, G.H., Li, Z., 2011. Sediment hosted Himalayan base metal deposits in Sanjiang region: characteristics and genetic types. Acta Petrol. Mineral. 30, 355–380 (in Chinese with English abstract).

Su, W.C., Heinrich, C.A., Pettke, T., Zhang, X.C., Hu, R.Z., Xia, B., 2009. Sediment-hosted gold deposits in Guizhou, China: products of wall-rock sulfidation by deep crustal fluids. Econ. Geol. 104, 73–93.

Tian, S.H., Ding, T.P., Mao, J.W., Li, Y.H., Yuan, Z.X., 2006. S, C, O, H isotope data and noble gas studies of the Maoniuping LREE deposit, Sichuan province, China: a mantle connection for mineralization. Acta Geol. Sin. 80, 540–549.

Trull, T.W., Kurz, M.D., Jenkins, W.J., 1991. Diffusion of cosmogenic ^3He in olivine and quartz: implications for surface exposure dating. Earth Planet. Sci. Lett. 103, 241–256.

Wang, F., He, M.Y., 2003. Lead and sulfur isotopic tracing of the ore forming material from the Baiyangping copper–silver polymetallic deposit in Lanping, Yunnan. Sedimentary Geology and Tethyan Geology 23, 82–85 (in Chinese with English abstract).

Wang, F., 2004. The genetic model of Baiyangping Ag polymetallic deposit, Yunman province. (Doctoral Report), Chengdu University of Science and Technology, Chengdu, p. 92 (in Chinese with English abstract).

Wang, G.H., 2010. The genetic model of Liancheng–Jinman vein-type copper in the Lanping basin, Yunman province. (Master Report), Kunming University of Science and Technology, Kunming, p. 77 (in Chinese with English abstract).

Wang, X.H., Hou, Z.Q., Song, Y.C., Yang, T.N., Zhang, H.R., 2011. Baiyangping Pb–Zn–Cu–Ag polymetallic deposit in Lanping basin: metallogenic chronology and regional mineralization. Acta Petrol. Sin. 27, 2625–2634 (in Chinese with English abstract).

Wei, J.Q., 2001. S–Pb Isotopic geochemistry of copper multi-metal deposits in Hexi, Yunnan province. Geology and Mineral Resources of South China 3, 36–39 (in Chinese with English abstract).

Whitney, D.L., Evans, B.W., 2010. Abbreviations for names of rock-forming minerals. Am. Mineral. 95, 185–187.

Wilkinson, J.J., 2001. Fluid inclusions in hydrothermal ore deposits. Lithos 55, 229–272.

Wu, N.P., Jiang, S.Y., Liao, Q.L., Pan, J.Y., Dai, B.Z., 2003. Lead and sulfur isotope geochemistry and the ore sources of the vein-type copper deposit in Lanping–Simao Basin, Yunan province. Acta Petrol. Sin. 19, 799–807 (in Chinese with English abstract).

Xiao, R.G., 1989. Reservation of thermal brine with ore-forming materials and abrupt mineralization. (Unpublished Postdoctoral Report), Institute of Geochemistry. Chinese Academy of Sciences, Guiyang, p. 77 (in Chinese with English abstract).

Xiao, R.G., Chen, H.Q., Shuai, K.Y., Yang, Z.F., 1994. Mineralization of the Jinman copper deposit in Mesozoic sedimentary rocks in Lanping, Yunnan Province. Geoscience 8, 490–496 (in Chinese with English abstract).

Xu, Q.D., Li, J.W., 2003. Migration of ore-forming fluids and its relation to zoning of mineralization in northern Lanping Cu-polymetallic metallogenic area, Yunnan Province: evidence from fluid inclusions and stable isotopes. Mineral Deposits 22, 365–376 (in Chinese with English abstract).

Xu, Q.D., Mo, X.X., 2000. Regional fluid characters and regimes of "Sanjiang" middle belt during Neo-Tethys. Acta Petrol. Sin. 16, 639–648 (in Chinese with English abstract).
Xu, Q.D., Zhou, L., 2004. Ore-forming fluid migration in relation to mineralization zoning in Cu-polymetallic mineralization district of northern Lanping, Yunnan: evidence from lead isotope and mineral chemistry of ores. Mineral Deposits 23, 452–463 (in Chinese with English abstract).
Xu, X.C., Xie, Q.Q., Lu, S.M., Chen, T.H., Huang, Z., Yue, S.C., 2005. Fluid inclusion characteristics of copper deposits on the western border of Lanping basin, Yunan Province. Acta Miner. Sin. 25, 170–176 (in Chinese with English abstract).
Xue, C.J., Chen, Y.C., Yang, J.M., Wang, D.H., 2002. Analysis of ore-forming background and tectonic system of Lanping basin, Western Yunnan Province. Mineral Deposits 21, 36–44 (in Chinese with English abstract).
Xue, C.J., Chen, Y.C., Wang, D.H., Yang, J.M., Yang, W.G., 2003. Geology and isotopic composition of helium, neon, xenon and metallogenic age of the Jinding and Baiyangping ore deposits, northwest Yunnan. Sci. China Ser. D 46, 789–800 (in Chinese with English abstract).
Xue, C.J., Chi, G.X., Chen, Y.C., Wang, D.H., Qing, H.R., 2006. Two fluid systems in the Lanping basin, Yunnan, China—their interaction and implications for mineralization. J. Geochem. Explor. 89, 436–439.
Xue, C.J., Zeng, R., Liu, S.W., Chi, G.X., Qing, H.R., Chen, Y.C., Yang, J.M., Wang, D.H., 2007. Geologic, fluid inclusion and isotopic characteristics of the Jinding Zn–Pb deposit, western Yunnan, South China: a review. Ore Geol. Rev. 31, 337–359.
Xue, W., Xue, C.J., Chi, G.X., Gao, B.Y., Yang, S.F., 2010. Study on the fluid inclusions of Baiyangping poly-metallic deposit in Lanping Basin, northwestern Yunan, China. Acta Petrol. Sin. 26, 1773–1784 (in Chinese with English abstract).
Yan, W., Li, C.Y., 1997. Geochemical characteristics and hydrothermal sedimentary genesis of a new type of copper deposits. Geochimica 26, 54–63 (in Chinese with English abstract).
Ye, X.R., Wu, M.B., Sun, M.L., 2001. Determination of the noble gas isotopic composition in rocks and minerals by mass spectrometry. Rock Miner. Anal. 20, 174–178 (in Chinese with English abstract).
Zhang, L.G., 1985. The Application of Stable Isotope to Geology. Shanxi Science and Technology Publishing House, Xi'an, p. 185 (in Chinese with English abstract).
Zhang, J.R., 2013. Spatial–temporal evolution of the ore-forming fluid and related mineralization in the western Lanping basin, Yunnan Province, China. (Doctoral Report), The University of Chinese Academy of Sciences, Guiyang, p. 105 (in Chinese with English abstract).
Zhang, C.J., Ni, S.J., Teng, Y.G., Peng, X.H., Liu, J.D., 2000. Relationship between Himalayan tectono-magmatic activity and mineralization in the Lanping basin. Miner. Petrol. 20, 35–39 (in Chinese with English abstract).
Zhang, Q., Shao, S.X., Liu, J.J., Liu, Z.H., 2002. Pb isotopic compositions and sources of the polymetallic ore deposits in the large ore cluster of Lanping Basin. Acta Miner. Sin. 22, 147–155 (in Chinese with English abstract).
Zhang, J.R., Wen, H.J., Qin, C.J., Wang, J.S., 2012. Fluid inclusion and stable isotopes study of Liancheng Cu–Mo polymetallic deposit in Lanping basin, Yunan Province. Acta Petrol. Sin. 28, 1373–1386 (in Chinese with English abstract).
Zhang, J.R., Wen, H.J., Qiu, Y.Z., Zhang, Y.X., Li, C., 2013. Ages of sediment-hosted Himalayan Pb–Zn–Cu–Ag polymetallic deposits in the Lanping basin, China: Re–Os geochronology of molybdenite and Sm–Nd dating of calcite. J. Asian Earth Sci. 73, 284–295.
Zhao, H.B., 2006. Study on the characteristics and metallogenic conditions of copper–polymetallic deposits in middle-northern Lanping basin, western Yunnan. (Doctoral Report), China University of Geosciences, Beijing, p. 123 (in Chinese with English abstract).